DENSE

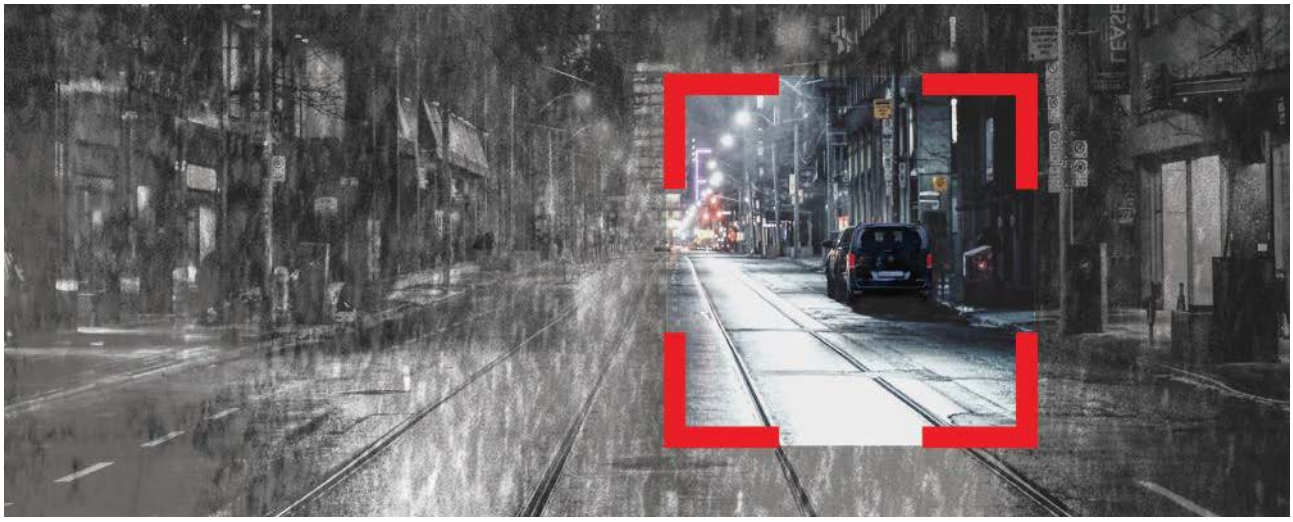

D2.1

Characteristics of Adverse Weather Conditions

Dissemination level PU

Version 1.0 Final

Lead contractor CER

Due date 30.09.2016

Version date 27.01.2017

Bundesministerium für Bildung und Forschung
Tekes
VINNOVA
Netherlands Enterprise Agency
ECSEL Joint Undertaking
Electronic Components and Systems for European Leadership
FLANDERS INNOVATION & ENTREPRENEURSHIP
Flanders State of the Art
Co-funded by the European Union

Document information

AUTHORS

Colomb Michèle - Cerema

Duthon Pierre - Cerema

Laukkanen Samuli - Vaisalsa

REVIEWERS

Jan-Erik Kallhammer - Autoliv

Hervé Illy- Renault

FUNDING

H2020-ECSEL-2015-1-RIA

Grant Agreement number: 692449

CONTACT

Dr. Werner Ritter

Daimler AG

Wilhelm-Runge-Straße 12

89082 Ulm

Germany

Phone: +49 731 505 2140

Email: Werner.R.Ritter@Daimler.com

www.DENSE247.eu

Revision log

Version	Date	Status	Author	Company
0.1	23-06-2016	D : draft proposal of content	Colomb	Cerema
0.2	22-07-2016	D : draft extended proposal of content	Colomb	Cerema
1.0	30-08-2016	RD : draft report to be reviewed (WP2 Workshop)	Colomb - Duthon	Cerema
1.1	06-09-2016	Input on Snow and road surface characteristics	Laukkanen	Vaisala
1.2	13-10-2016	RD : draft including "characteristics of spray" to be reviewed	Colomb-Duthon	Cerema
2.0	02-11-2016	RD : reworked draft	Colomb-Duthon	Cerema
2.1	06-11-2016	Autoliv Review	Kallhammer	Autoliv
2.2	14-11-2016	Added introduction by Renault and Review	Illy	Renault
2.3	25-11-2016	RD : reworked draft	Colomb - Duthon	Cerema
	02-12-2016	RD : reworked draft	Laukkanen	Vaisala
2.4	11-01-2017	RD : complementary comments	Kallhammer	Autoliv
2.5	23-01-2017	RD : reworked draft	Colomb-Duthon	Cerema
2.6	26-01-2017	Renault Review	Illy	Renault
2.7	27-01-2017	RD : reworked Final draft	Colomb	Cerema

Table of contents

List of figures

List of tables

1 Executive summary

This report describes the natural characteristics of adverse weather that may affect the driving conditions: fog, rain, road icing and snow, and the physics that can affect the response of the sensors used for advance driving assistance and future autonomous vehicles. In order to develop the most efficient sensor suite in the DENSE project, it is required to have a deep knowledge of the natural characteristics of adverse weather conditions. After an extensive bibliographical survey of each condition, the available methods to reproduce in controlled conditions fog and rain will be presented.

The chapter related to fog characteristics gives first the physical definition of fog, with a summary of fog types considered by weather services, in relation to fog formation mechanisms and fog live cycle. Six types may be considered. The two types that are most frequently encountered "Radiation fog", also described as "Continental fog", and "Advection fog" described as "Maritime fog". In driving conditions, impact of fog on the visibility and the ability to detect obstacles can be explained mainly by the attenuation of energy beam by droplets, and, in a secondary effect, by scattering. In the transport domain, the macroscopic parameter used is the meteorological visibility (meters). Fog is defined for visibility less than 1000 m. "Road fog" critical for driving has visibility less than 400 m. This definition is given for visible radiations. Spatial and seasonal variation of fog occurrence in European territory is described. The microphysical properties of fog are addressed as the visibility is closely related to the droplet size distribution by the extinction coefficient. A huge amount of experimental studies gives an overview of the variety of natural fog. Some parameterisation is proposed but these models are limited to the visible bandwidth, under the scope of DENSE project. The bandwidth of the DENSE project is the SwIR bandwidth. However, the amount of scientific literature dedicated to the description of the impact of bad weather conditions like fog in SwIR bandwidth is limited because the physics is not yet well known. Some references provide very useful information but still limited. Hence, only few words about these studies are given in this report. It is in the scope of the validation phase of the project (WP6) to describe in more details the impact of physics. In the last part of this chapter, the fog observation techniques and available sensors are presented, both for visibility and droplet size distribution measurements.

In driving conditions, impact of rain on the visibility and the ability to detect obstacles can be explained mainly by four effects: the transmission through the atmosphere, the reduction of visibility by the water on the windscreen, the effect of water on the road surface and also the production of spray by the tires behind the vehicle. The impact of wavelength on radiation transmission through the atmosphere is discussed. Some studies show the effect of various rain intensities (and fog) on the atmospheric attenuation, from radiation wavelength from 0.3 µm to 3 cm. The heaviest and heavy rain may affect more than fog, the sub-millimetre waves. This is the challenge of the DENSE project to find a sensors suite with data fusion, operating in all weather conditions. The macroscopic parameter describing the rain intensity is the rainfall rate (mm/h). Four ranges of intensities are defined by a standard (Very light, Light, Moderate, and Strong). Some figures of the microphysical parameters (drop size distribution) and fall velocity of drops are given. The rain sensors are rain gauge, (for rainfall rate) and rain disdrometer (for drop characteristics).

DENSE project also considers ice and snow conditions. Snow is characterized by three level of snowfall intensity (Light, Moderate, and Heavy). A new generation of sensors, "Present weather sensors" can

discriminate snow precipitation from other phenomena as fog, rain, or hail. The atmosphere is affected by the snow fall that reduces visibility, but the winter conditions affect also the road surface state. Some standard discriminates 5 surface states (Dry, Moist, Wet, Streaming water, Slippery). They influence the friction between vehicle tire and road surface. Stationary and mobile sensors are available. In DENSE project, the integration of optical remote sensor in the vehicle will be examined.

A state of the art of available solutions to simulate rain and fog will be presented. Thermodynamical or mechanical processes and corresponding infrastructures are described. In the field of transport, only one infrastructure by continent is identified. In Europe, the French Cerema R&D platform will be used both for fog and rain simulation. Some upgrade of the rain system will be undertaken in the DENSE project.

2 Introduction

Compared to normal conditions, bad weather conditions reduce the perception of the environment around the vehicle. To a first approximation, the main effect is a decrease in the range visibility that can be very critical in a driving context.

This phenomenon is due to a change in the optical properties of the atmosphere. Several physical mechanisms are involved, mainly scattering and attenuation. The physics underlying these phenomena is based on a complex interaction between the beam propagation (light, laser, electromagnetic) and the microscopic structure of the atmosphere.

However, the aim of this report is not to describe in detail this interaction but to define the key parameters that can define the atmosphere in such conditions. One of the challenges is to be able to detail a generic description of atmosphere that allows covering the huge amount of bad weather conditions met in real conditions. The approach is based on a state-of-the-art of the physical characteristics of natural hydrometeors (rain, fog and snow).

This description is useful for:

- the specifications and the development of the sensor suite
- the validation and evaluation phase of the system

3 Fog

3.1 Fog physics

3.1.1 Fog definition

In the meteorological glossary of the American Meteorological Society, AMS (Glickman & Zenk, 2000), fog is defined as suspended droplets in vicinity of the earth's surface that reduces the visibility below 1 km. The online AMS glossary provides also a more comprehensive definition of fog, which introduces several important terms for which simple definitions are also provided. We find this definition useful and cite it here: *"According to an international definition, fog reduces visibility below 1 km (0.62 miles). Fog differs from cloud only in that the base of fog is at the earth's surface while clouds are above the surface. When composed of ice crystals, it is termed ice fog. Visibility reduction in fog depends on concentration of cloud condensation nuclei and the resulting distribution of droplet sizes. Patchy fog may also occur, particularly where air of different temperature and moisture content is interacting, which sometimes make these definitions difficult to apply in practice. Fogs of all types originate when the temperature and dew point of the air become identical (or nearly so). This may occur through cooling of the air to a little beyond its dew point (producing advection fog, radiation fog or upslope fog), or by adding moisture and thereby elevating the dew point (producing steam fog or frontal fog). Fog seldom forms when the dew point spread is greater than 2°C. According to U.S. weather observing practice, fog that hides less than 0.6 of the sky is called ground fog. If fog is so shallow that it is not an obstruction to vision at a height of 2 m above the surface, it is called simply shallow fog. In aviation weather observations fog is encoded F, and ground fog GF. Fog is easily distinguished from haze by its higher relative humidity (near 100%, having physiologically appreciable dampness) and grey colour. Haze does not contain activated droplets larger than the critical size according to Köhler theory. Mist may be considered an intermediate between fog and haze; its particles are smaller (a few micrometre maximum) in size, it has lower relative humidity than fog, and does not obstruct visibility to the same extent. There is no distinct line, however, between any of these categories. Near industrial areas, fog is often mixed with smoke, and this combination has been known as smog. However, fog droplets are usually absent in photochemical smog, which only contains inactivated haze droplets."*

In the "Meteoterm" terminology database of the World Meteorological Organization (WMO, 2016), fog is defined as the "Suspension of very small, usually microscopic water droplets in the air, generally reducing the horizontal visibility at the Earth's surface to less than 1 km". The Meteoterm database does not provide a more comprehensive definition.

Thus, it is worth noting that there are two aspects of defining fog. On one hand, it is defined using the visibility threshold of 1 km; however, this does not distinguish the phenomenon causing the drop in visibility. On the other hand, fog is defined in a physical way, by specifying that the drop in visibility is caused by the presence of small, but activated droplets, as opposed to smoke or haze where the particles are not activated (see section 3.3 for details) and to the larger droplets or snowflakes that may reduce visibility in heavy rain or blowing snow. Both the visibility threshold and the physical specification is needed to properly distinguish fog from other meteorological phenomena.

Finally, it is worth noting that these definitions only concern the liquid phase of water. However, fog containing ice crystals also occurs. It can then be referred to as ice fog (contains only ice crystals) or mixed-phase fog (contains both ice crystals and droplets) (Glickman & Zenk, 2000; Ismail Gultepe et al., 2007). Gultepe et al. (2007) give an approximate temperature threshold of -10 ˚C for the appearance of mixed-phase fog and -20 to -30 ˚C for ice fog. In freezing fog, the fog is composed of liquid droplets, but the droplets will freeze at the contact of an exposed object (Glickman & Zenk, 2000). Freezing fog typically occurs when the temperature decreases gradually below 0 ˚C (Ismail Gultepe et al., 2007). The following presentation of fog will mainly focus on the liquid fog, since this is the most relevant for most of Europe; however, some specifications regarding ice fog will be given.

3.1.2 Fog formation

There are several meteorological phenomena that can cause fog to appear. To form a fog, the air near the surface needs to become supersaturated, that is containing more water vapour than it can hold on to and hence causing droplets to form. As warm air can hold on to more vapour than cold air, saturation may be reached either by cooling or moistening of the air.

Fog types can be defined according to the mechanism of formation. An overview of these fog types is given in the review paper by Gultepe et al. (2007), and largely based on this paper a brief presentation of some important fog types will be given in the following. A summary is presented in Table 3.1.

Table 3.1: Summary of fog types and their formation mechanisms. See text for details.

Fog type	Mechanism
Radiation fog	Radiative cooling of the surface under clear sky
Advection fog	Moist, warm air flowing over water with different temperature
Steam fog	Very cold air flowing over much warmer water
Stratus-lowering fog	Gradual lowering of the base of a low cloud down to the surface
Precipitation fog	Evaporation of precipitation, mixing of air-masses at a warm front
Upslope fog	Adiabatic cooling of air being forced to lift by the topography

Radiation fog forms when the surface is cooled to dew point due to radiative cooling, usually under clear sky during night. This type occurs frequently in continental climates under anticyclonic (high pressure conditions) conditions during winter (Avotniece, Klavins, & Lizuma, 2015; e.g. Haeffelin et al., 2010). For this fog type to form, there should not be too much wind, allowing saturation and droplets to form in the air close to the surface (e.g. Zhou & Ferrier, 2008). However, if the conditions are too calm, it may result in dew forming on the surface instead, because some turbulence is needed for the cooling of the surface to be transmitted into the air (Haeffelin et al., 2013).

A recent review of marine fog is given by Koračin et al. (2014): *Advection fog* forms when warm, humid air flows over a large body of water with lower temperature, causing the air to cool to saturation. It is a common phenomenon in coastal regions of mid-latitudes, especially where there are upwelling of cold water. Conversely, advection fog can also be formed when cold air with high relative humidity flows over a

warmer sea surface; vertical mixing then causes supersaturation of the air. In high latitudes or above lakes in wintertime, the air can typically be much colder than the water, and this gives rise to a phenomenon referred to as *steam fog*.

Fog can also form by the gradual lowering of a pre-existing stratus cloud. The mechanism for the cloud-base lowering can be the radiative cooling of the cloud top, the moistening of the air below the cloud through mixing with the cloud or evaporation of falling drizzle, and large-scale subsidence of the air-mass (J.-C. Dupont et al., 2012; e.g. Koračin et al., 2014).

Fog can also occur associated with precipitation events, often associated with the passage of a warm front. The mechanism can be the saturation of the air by evaporating precipitation or the mixing of the warm and cold air mass which meet at the front. Gultepe et al. (2007) call this fog type *frontal fog*. Tardif and Rasmussen (2007) use the term *precipitation fog* for all fog forming during precipitation.

When an air mass is forced to lift due to the topography, it will cool adiabatically and can thus reach saturation. This causes frequent fog formation on the upwind side of hills and mountain ranges, especially when the wind is blowing from a source of moisture (Błaś, Sobik, Quiel, & Netzel, 2002).

An objective method for distinguishing some of the common fog types based on ground meteorological observations (temperature, wind speed, precipitation, and cloud-base height) is given by Tardif and Rasmussen (2007).

3.1.3 Fog life cycle

Once fog has formed, its further development or dissipation will depend on the evolution of its environmental conditions and the physical processes that govern the production and removal of liquid water.

To maintain the fog, a source of continued cooling or moistening of the air is needed in order to provide liquid water. This can typically be the radiative cooling at the top of the fog, which can be affected by a change in the atmosphere above the fog; for example, it will be reduced by the appearance of a higher cloud (J.-C. Dupont et al., 2012). When the fog formation mechanism is related to the advection of a moist air mass, as in advection fog and upslope fog, the persistence of the fog will therefore also be affected by changes in the wind speed, wind direction and air mass source (Koračin et al., 2014).

Several processes cause the fog to lose liquid water. The sedimentation (droplets falling due to their size) transports water towards the ground, where it is deposited by turbulence (e.g. Zhou & Ferrier, 2008). Since the radiative cooling occurs near the fog top, the fog layer will become unstable, causing up- and downdrafts to appear, which mix the fog layer vertically (Nakanishi, 2000). In fact, these downdrafts can transport the liquid water towards the surface and decrease the visibility there (Bergot, 2016). Turbulence near the fog top will also cause mixing of the foggy air with drier air from above the fog, causing evaporation of the droplets (Ismail Gultepe et al., 2007). The presence of turbulence is thus considered mainly a mechanism which breaks down the fog. Radiation fog will often be in a state of equilibrium between the sources and sinks of liquid water (e.g. Price, 2011; Zhou & Ferrier, 2008).

Solar radiation can be important for the dissipation of fog over land. The solar radiation heats the ground, which then transfers this heat to the fog through the turbulent sensible heat flux, causing the fog to evaporate from below (Haeffelin et al., 2010). The fog droplets will also absorb some of the solar radiation directly, causing heating and evaporation within the fog layer (e.g. Nakanishi, 2000). This is why fog often forms during the night and dissipate during the morning, in particular radiation fog (e.g. Tardif & Rasmussen, 2007). It is worth noting that fog dissipation does not always involve a complete disappearance of the fog cloud. Often the surface visibility increases because the fog base lifts, turning the fog into a stratus cloud (e.g. J.-C. Dupont et al., 2012).

Fog may also be evolving due to non-local mechanisms. It may be formed at one place and then transported by the prevailing winds to somewhere else. Price et al. (2011) showed that fog can also spread out horizontally through the mixing of clear and cloudy air occurring at the horizontal boundary of the fog.

The duration of a fog can be very variable from case to case. Sometimes the fog forms in small patches that does not even last for one hour. Tardif and Rasmussen (2007) find in their climatology for New York that a well-developed fog will typically last for 5-10 hours, while in some cases it can last for as much as 24 hours. The duration will depend on the persistence of synoptic conditions favourable to the fog. For radiation fog, the duration is typically limited due to sunrise.

3.2 Macroscopical parameters

3.2.1 Visibility theory

The AMS glossary defines visibility as follows: "The greatest distance in a given direction at which it is just possible to see and identify with the unaided eye 1) in the daytime, a prominent dark object against the sky at the horizon, and 2) at night, a known, preferably unfocused, moderately intense light source" (Glickman & Zenk, 2000).

On the road, there are two approaches to calculate the visibility, based on the two definitions above: the visibility by contrast, and the visibility of a light source. The visibility by contrast is the most relevant in most cases (for the visibility of signs, road markings and obstacles against the background, which is illuminated either by daylight or by street- and headlights), while the visibility of a light source is mainly relevant for seeing the lights of another vehicle.

<u>Visibility by contrast:</u>

The theory of Koschmieder describes the apparent contrast of an object against the horizon (Hautière, Tarel, Lavenant, & Aubert, 2006): The total luminance L reaching the observer from an object at distance d through a diffusing media (e.g. fog) with an extinction coefficient β (m^{-1}) is:

$$L = L_0 e^{-\beta d} + L_f \, (1 - e^{-\beta d})$$

Where L_o is the luminance of the object at close range and L_f is the luminance of the horizon. The first term is the light from by the object itself, while the second term is the diffuse light from the environment which has been scattered into the vision of the observer. Thus, as the distance increases, the observer will see

less and less of the light from the object, and more and more of the diffused from the environment light. This causes a decrease in the contrast between the object and its background, which is described by the law of Duntley (Babari, 2012; Hautière et al., 2006):

$$C = \frac{L - L_f}{L_f} = C_0 e^{-\beta d}$$

Where C is the contrast between the object and the background at distance d, and C_o is the contrast at close range. Figure 3.1 illustrates this decrease of contrast with distance and atmospheric extinction.

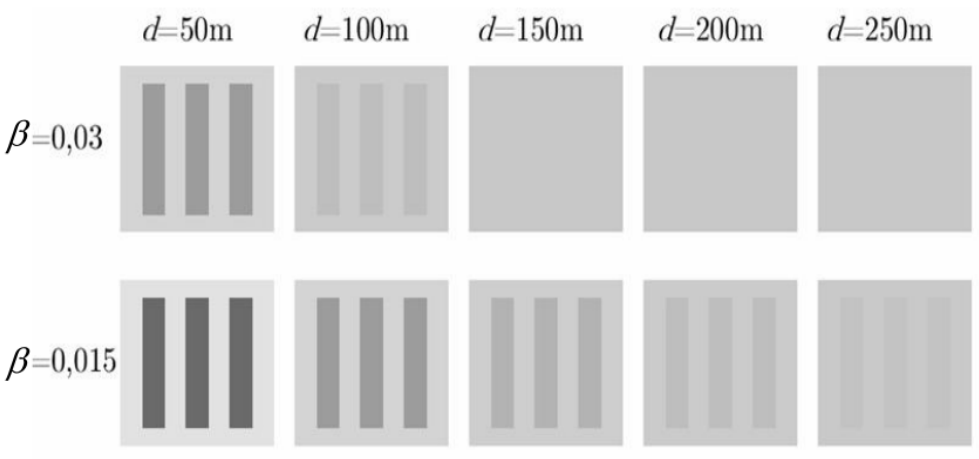

Figure 3.1: Illustration of how the contrast between an object and its background decreases with distance d and the atmospheric extinction coefficient β. From Babari (2012).

C_o will in general depend on the object and its background. However, to define a standardized visibility, a black object against a white horizon is assumed, giving a C_o of 1. Furthermore, a threshold of contrast of 0.05 (5 %) is assumed to be the limit of what the eye can distinguish. By solving Duntley's equation for d under these assumptions, we get Koschmieder's formula for visibility distance (Babari, 2012):

$$\mathrm{Vis} = -\frac{\ln 0.05}{\beta} \approx \frac{3.0}{\beta}$$

This visibility formulation is referred to as the "meteorological visibility distance" by Hautière et al. (2006). Originally, Koschmieder set this constant to 0.02 (i.e. only 2 % contrast is needed for an object to be visible), which gives Vis=3.9/β (Horvath & Noll, 1969; Kunkel, 1984). However, today both the International Commission on Illumination (CIE) (Dumont, 2002) and the WMO (Li & Peng, 2012) uses the 5 % threshold to define the meteorological visibility.

Although the Koschmieder theory depends on several assumptions (e.g. static and uniform atmosphere, flat and diffuse ground surface, the observed object is small compared to the distance to the observer), the law is a good approximation (Babari, 2012), and the visibility-extinction relationship has been verified by simultaneous observations (Horvath & Noll, 1969).

Since the contrast of an object at close range will often be less than the standardized black-white, the true visibility distance of an object may be less than the meteorological visibility. While Koschmieder's formula gives a visibility distance which is independent of the object, the more general Duntley's law can be used to calculate the distance at which a particular object having $C_0 < 1$ is lost from view (the distance *d* at which C=0.05).

Visibility of a light source:

The law of Allard is used for the visibility of light sources. It describes the illuminance E reaching the observer from a light source with luminous power I as function of distance d and atmospheric extinction β (Babari, 2012):

$$E = \frac{Ie^{-\beta d}}{d^2}$$

That is, the initial light intensity is attenuated by the atmospheric extinction β (as in Koschmieder's law above), but also because the energy from the source is spread over an increasing spatial surface (proportional to d^2). This formula is used to calculate the night-time visual range of light sources, which is the value of *d*, which gives a critical threshold illuminance E_c visible to the eye (Babari, 2012).

At airports, the runway visual range (RVR) is the distance at which the pilot can see the markings at the landing runway, and it is an important measure for the safe landing and take-off. At night, or when the atmosphere is opaque, the Law of Allard is used for the visibility of the luminous markings of the runway.

Other aspects of visibility on the road

The term "mobilized visibility" is used for the distance to the furthest visible object on the road (Hautiere, Labayrade, & Aubert, 2006). Depending on the availability of contrasted objects along the road, this distance can be smaller or equal to the general visibility distance defined above (Figure 3.2).

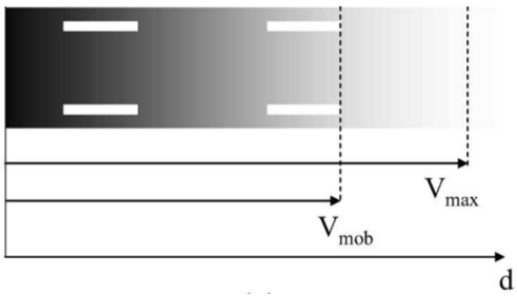

Figure 3.2: The mobilized visibility (Vmob) is the distance to the most distant visible object actually existing on the road, while the (general) visibility (Vmax) is the longest distance at which the object would be visible. From Hautière et al. (2006).

The French norm NF P 99-320 (AFNOR, 1998) defines road fog by visibility below 400 m, divided into 4 classes, as presented in Table 3.2. Thus, a road fog has a lower threshold of visibility than a meteorological fog (1 km). This norm also specifies that the visibility measures be taken at 1.20 m above the ground.

Table 3.2: Definitions of fog classes from the AFNOR norm NF P99-320 (April 1998)

	Road visibility class	Visibility distance (m)
Meteorological fog		< 1000
Road fog	1	200 to 400
	2	100 to 200
	3	50 to 100
	4	< 50

Summary: Visibility theory

The visibility is defined to correspond to the human capacity to see objects at distance. The visibility by contrast will in general depend on the close-range contrast of the object to be observed towards the background as well as the properties of the atmosphere; however, to standardise the quantity, a black object against a white background is used to define the meteorological visibility. This visibility distance is well approximated as being inversely proportional to the atmospheric visible extinction coefficient (Koschmieder's equation). For the visibility of light sources at night, the radiance of the source should also be taken into account (Allard's law).

In the remainder of Section 3, discussions about visibility in fog will always refer to meteorological visibility.

3.2.2 Fog occurrence in Europe

This section presents available knowledge of the occurrence of fog in Europe. In the first part, the fog frequency of the latest decades and its geographical and seasonal variations are presented. In the second part, we briefly discuss the decrease in fog frequency that has been observed in Europe over the last decades.

Spatial and seasonal variations of fog occurrence:

Figure 3.3 shows the number of days in summer and winter with occurrence of visibility below 200 m (dense fog) and below 2 km (fog or mist) for a large number of locations in Europe, as a mean for the period 1976-2006. This figure, taken from the study of van Oldenborgh et al. (2010), thus gives a general idea of the spatial and seasonal variability of fog occurrence. There is generally much more fog in Northern Europe than in the Mediterranean region. The Alps and Eastern Europe have particularly high occurrence of fog, while Ireland and the west coast of Great Britain have rather low occurrence. The winter is usually foggier than the summer, especially at inland sites, where radiation fog is often a dominating fog type, e.g. Swiss plateau (Scherrer & Appenzeller, 2014) or Po Valley in Italy (Giulianelli et al., 2014). The number of days with occurrence of visibility below 200 m per half-year varies from >15 days during winter in the Alps and parts of Eastern Europe to <3 days in many places during summer and at most Mediterranean sites both in summer and winter.

The contrast between the Mediterranean and Northern Europe in low cloud cover can also been evidenced by satellite studies (Cermak, Eastman, Bendix, Warren, & others, 2009). However, satellite studies are not directly applicable to fog because they cannot easily distinguish fog events from low stratus clouds (because the cloud base altitude must be calculated from estimates of cloud-top height and cloud thickness, which have uncertainties) (Cermak & Bendix, 2011).

There is also evidence for an urban-rural gradient in fog frequency. Sachweh and Koepke (1995) found that the cities in South Germany were exposed to less fog than the surrounding areas. They explained it by the urban heat island effect in post-industry cities. This effect was also found by Tardif and Rasmussen (2007) for New York city.

Vajda et al. (2011) is a report for the EU FP7 on the weather hazard impacts on transportation. They studied the occurrence of visibility below critical thresholds for aviation safety on several airports in Europe (Figure 3.4). The thresholds considered were 550 m, 300 m and 200 m (the actual definitions also depend on the cloud-base height). It can be seen that the airports along the Mediterranean have much less dense fog occurrence than the rest of Europe, while the Po Valley (Milan) and Switzerland are most exposed.

Several studies have been performed on fog occurrence in different locations in Europe, and here we mention some of them:

- Scherrer and Appenzeller (2014) studied fog climatology on the Swiss plateau; here the fog shows a strong seasonality with most of the fog occurring October-February and a total of ~30 fog days per year.
- According to Błaś et al. (2002), the mountain ranges in Western and Central Europe are heavily exposed to fog (mainly upslope fog), when winds are coming from the Atlantic Ocean. Many sites above 1000 m have fog more than 50 % of the days of the year. Błaś et al. (2002) present a climatology of fog in Sudety Mountains (Poland).
- Giulianelli et al. (2014) present a climatology of fog in Po Valley (North Italy), which is an area where fog occurs frequently, especially during fall/winter, and where 30 % of the Italian population lives.
- Avotniece et al. (2015) present a climatology of fog occurrence in Latvia (52-year period). They report 19-59 fog days per year (variability among 14 stations), with two seasonal peaks: September-December (radiation fog) and March-May (advection fog from the Baltic Sea).

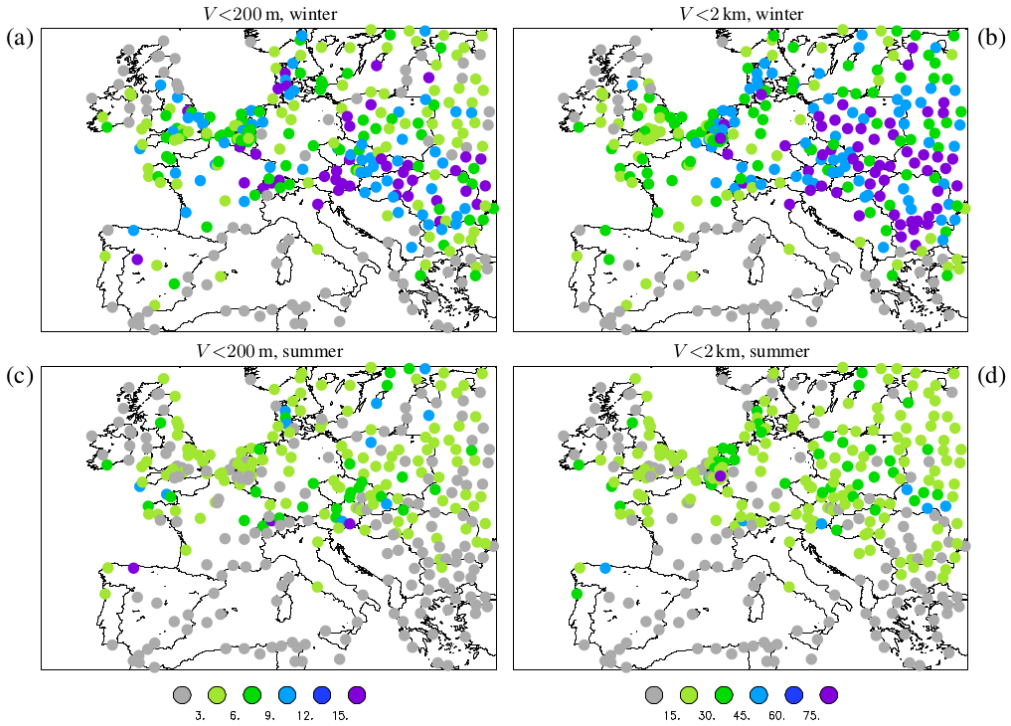

Figure 3.3 : The mean number of days per half-year in 1976-2006 when visibility below 200 m (left) and 2 km (right) occurred (NB: different colour scale); for October-March (top) and April-September (bottom). From van Oldenborgh et al. (2010).

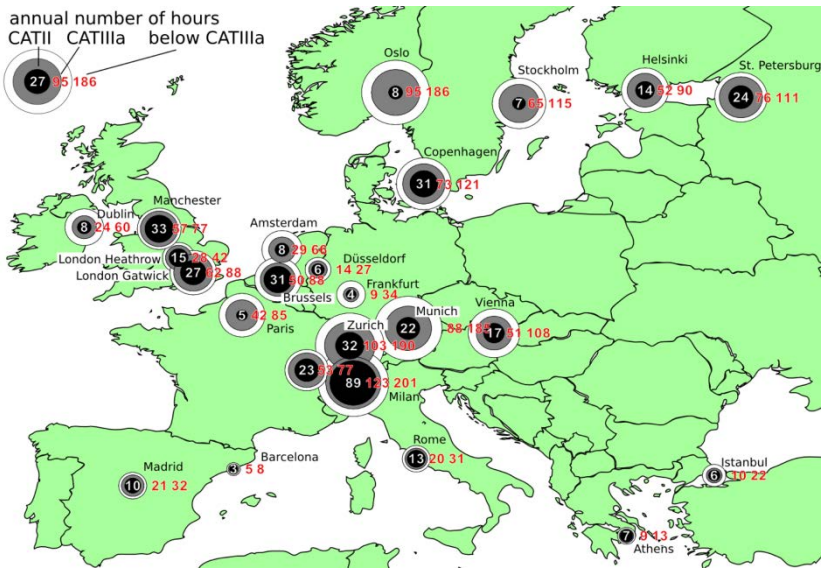

Figure 3.4: Number of hours per year (2000-2009) with low visibility at some European airports, for 3 levels of reduced visibility (below 550 m, 300 m and 200 m). From Vajda et al. (2011).

A decreasing trend in fog frequency:

A decrease in low visibility events has taken place all over Europe since the 1970s. Vajda et al. (2011) report a decrease of more than 50 % (from the 1970s to the 2000s) of the number of hours with very low visibility at the European airports shown in Figure 3.4. Figure 3.5 shows the trends in occurrence of visibility below 200 m and 2 km, found by van Oldenborgh et al. (2010). The orange and red dots mark mark where a strong decrease in fog frequency has taken place during 1976-2006. This means that the amount of fog at these locations has been considerably less in the latest years than what is shown in Figure 3.3, which shows the mean of the whole period 1976-2006. However, there are also locations where fog frequency has only weakly decreased or not at all. Overall, van Oldenborgh et al. (2010) finds a decrease of ~50 % of the occurrence of visibility below 200 m in large parts of Europe, while Vautard et al. (2009) report a 50 % decrease in occurrence of fog or mist (visibilities below 2 km) at measuring sites throughout Europe. Vautard et al. (2009) suggest the decrease is related to the reduction in sulphur dioxide emissions (which is efficient at producing CCN (see section 3.3). However, the reduction in low visibility occurrence has been weaker since 2000; Vautard et al. (2009) explains this by the air quality policies already having reduced the emissions to a low level, so that the low visibility occurrence should not be expected to decrease further in the future. On the other hand, Klemm and Lin (2016) argue that temperature increase (due to climate change) also can be a mechanism for reducing fog occurrence.

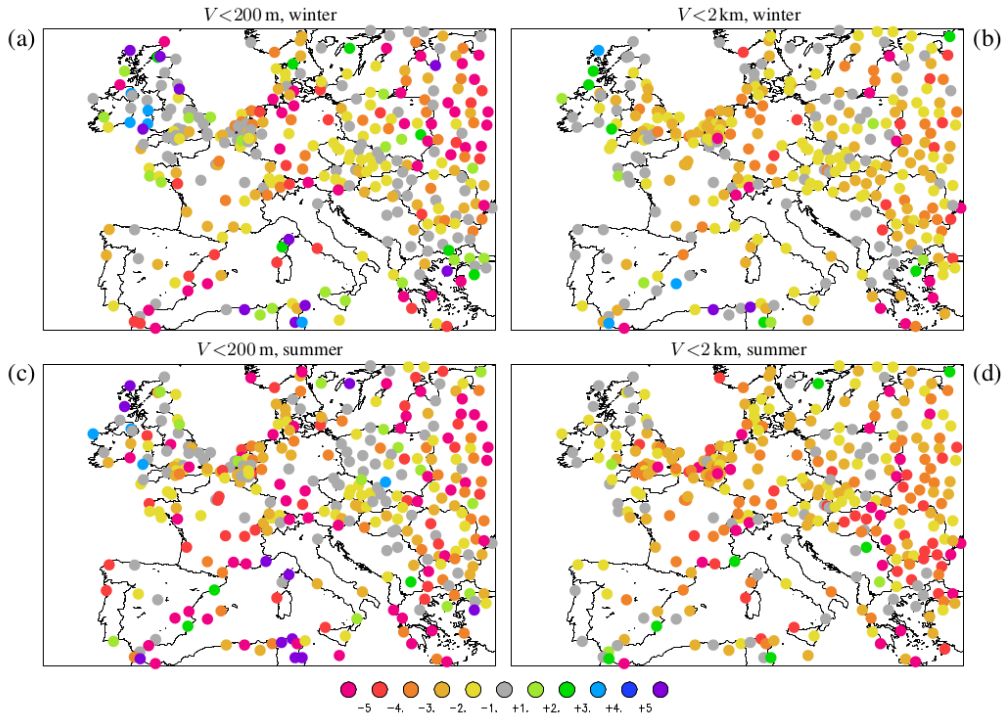

Figure 3.5: The relative trend (%/year), over the period 1976-2006, in the number of days per half-year when visibility below 200 m (left) and 2 km (right) occurred; for October-March (top) and April-September (bottom). The relative decline is defined relative to the mean value over the period (Figure 3.3); a trend of -3 %/yr corresponds to the number of days being halved during the 30-year period, while a trend of -5.5 %/yr means that low visibility no longer occurs at the end of the period. From van Oldenborgh et al. (2010).

Summary: Fog occurrence in Europe

Fog occurs frequently in many areas across Europe, in particular in the winter, but much less often in the Mediterranean region. The cities experience less fog than rural areas due to the urban heat island, while mountainous areas can be heavily exposed to fog due to upslope winds. The number of fog days has decreased significantly since the 1970s, most likely due to reduction in air pollution. Whether this decrease will continue in the future is uncertain, as it may be affected by climate change as well as air pollution.

3.3 Microphysical parameters

3.3.1 Theory of fog microphysics

In this section, we will introduce the basic mechanism of droplet formation, and then the concept of the droplet size distribution and its relation to the extinction by fog in the visible and the infrared.

Formation of fog droplets

In the population of suspended particles in the atmosphere (aerosols), certain particles are soluble in water, depending on their chemical composition (Rogers & Yau, 1996). When the atmospheric relative humidity approaches 100 %, these particles will grow by taking up water from the atmospheric vapour (deliquescence). However, their growth is limited to sizes of ~1 µm until they are activated into droplets. For this activation, a certain amount of supersaturation (relative humidity above 100 %) is necessary due to the energy required to create the droplet surface area (Rogers & Yau, 1996). Depending on the mass and composition of the dry aerosol particle, this activation occurs at a certain critical size and requires the supersaturation to exceed a critical value. Once activated, the particles will grow spontaneously whenever the air is supersaturated, and they are termed droplets. The aerosols capable of forming droplets through this process are called cloud condensation nuclei (CCN) (Rogers & Yau, 1996). The CCN that have not passed the critical size of activation will not grow spontaneously, and they are referred to as inactivated (or haze particles) (Glickman & Zenk, 2000).

The initial population of droplets evolves due to condensational growth, collision and coalescence of droplets, the evaporation of droplets in unsaturated intrusions into the cloud/fog and the gravitational settling of big droplets (Rogers & Yau, 1996 ch. 7). The sizes of the droplets can therefore vary during the life cycle of a fog, and in the vertical.

Droplet size distribution terminology:

The droplet size distribution (DSD) is represented mathematically by the function *n(D)*, describing the concentration of droplets (number per cm^3) of diameter *D* (more precisely, *n(D)* is the concentration of droplets in a narrow size interval around *D* divided by the width of this size interval, so its unit is $cm^{-3}\mu m^{-1}$). (NB: Sometimes the DSD is presented as function of the droplet radius (half of the diameter) instead.)

The total number of droplets is:

$$N = \int_{D_{min}}^{\infty} n(D)dD$$

The minimum size to include, D_{min}, separates the droplet population from the inactivated aerosols. It is not obvious where to set the D_{min}, since aerosols activate into droplets at different sizes depending on their chemistry and mass (Mazoyer, 2016; Rogers & Yau, 1996). The droplet number concentration found in observational studies can therefore be sensitive to the lower threshold that has been used. This lower threshold is typically set to a value in the range 1-4 µm. Actually, the large number of inactivated aerosols that have attained sizes of ~1 µm by deliquescence may contribute significantly (20 %) to the extinction of visible radiation during fog (Elias et al., 2009, 2015).

The upper size limit for fog droplets is not very clear either. When the droplets are large enough to fall with a significant speed, we term them drizzle drops (Glickman & Zenk, 2000). The terminal fall speed of droplets increases rapidly with size, from about 1 cm/s for diameter 20 µm to 7 cm/s for 50 µm and 27 cm/s at 100 µm (Rogers & Yau, 1996). However, the conventional border between cloud drops and drizzle drops is not before 200 µm (and it is called a raindrop above 500 µm) (Glickman & Zenk, 2000). On the other hand, most instruments that measure the DSD stop at around 50 µm (section 3.4). Due to collision growth, fog clouds may produce light drizzle that falls to the ground (e.g. J.-C. Dupont et al., 2012).

The total liquid water content of the foggy air (LWC, g/m^3) is found from the third moment of the DSD:

$$LWC = \int_{D_{min}}^{\infty} \frac{\pi \varrho_w}{6} n(D)D^3 dD$$

(ϱ_w is the density of liquid water) and the total surface area (m^2/m^3) is found from the second moment:

$$S = \int_{D_{min}}^{\infty} \pi\, n(D)D^2 dD$$

The effective (or equivalent) diameter relates the LWC and the total surface area:

$$D_{eff} \equiv \frac{\int_{D_{min}}^{\infty} n(D)D^3 dD}{\int_{D_{min}}^{\infty} n(D)D^2 dD} = \frac{6\, LWC}{\varrho_w S}$$

The effective diameter is thus a measure of a typical size in a population of droplets; more precisely it is the diameter that the droplets would have if they all were identical, in order to give the same surface area and the same LWC as the actual DSD (but not the same number of droplets). The effective diameter will typically be larger than the mean diameter (sum of all diameters divided by the number of droplets). The effective diameter is useful when considering the radiative effects of fog, because the radiative properties are mainly sensitive to the surface area of the droplets (Hu & Stamnes, 1993). This will be discussed further below. NB: The effective radius is simply half of the effective diameter.

A technical remark: The DSD is often presented on a logarithmic size scale (e.g. in plots). Then the quantity shown is actually the number concentration within a *logarithmic* size interval, and the integrals for calculating *LWC*, D_{eff} etc. must then be taken in the log-space (*d(log D)* instead of *dD*).

The size distribution is also used when studying ice crystals. Since the ice particles are not spherical, the size parameter must be defined differently and according to the usage. For example, it can be defined as the diameter if it melted (relevant for the ice water content) or as the largest linear dimension of the crystal (relevant for fall speed) (Rogers & Yau, 1996).

Parameterisation of the droplet size distribution:

The DSD is parameterised using mathematical functions. While the log-normal distribution (Heintzenberg, 1994) is often used for aerosols, the modified gamma distribution is a good choice for the fitting of droplet size distributions in both fog and other clouds (Tampieri & Tomasi, 1976). The mathematical form of the modified gamma distribution is (describing the distribution as function of radius *r*):

$$n(r) = a\, r^{\alpha} \exp[-\frac{\alpha}{\gamma}(\frac{r}{r_c})^{\gamma}]$$

where the parameters α and γ describe the slope of the distribution, while r_c is the radius where the distribution has its mode (peak). *a* is a factor proportional to the number concentration.

An example of the fitting of the distribution of observed data is shown in Figure 3.6. The fitting of the distribution depends on the sensor characteristics.

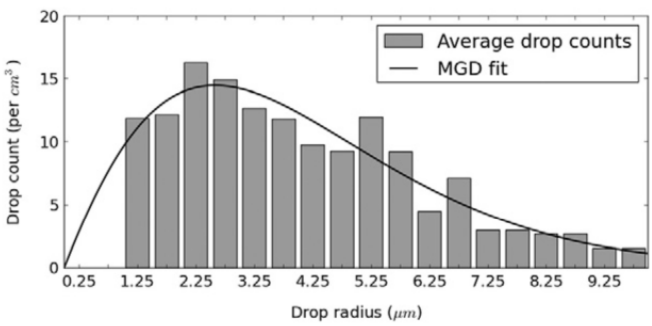

Figure 3.6: An example of the fitting of the modified gamma distribution to an observed droplet size distribution. The parameters in this case are rc = 2.58 µm, γ = 1.37, a = 11.63 and α = 1. From (Egli, Maier, Bendix, & Thies, 2015).

The same fog measured by sensors having various sampling range (0.5 to 15µm or 2 to 50 µm), may have various parametrisation. (see the same fog measured by various sensors (see 3.4.2 - Instruments measuring microphysical characteristics, Figure 3.16). The sensor (Fog monitor) with a sampling range beginning at 2 µm couldn't find the first peak (mode) at about 1 µm of this natural distribution that seems to be bimodal, with the peek diameter changing from beginning to the end of the fog formation. (Tampieri & Tomasi, 1976) shows that for bimodal distributions it is also possible to fit a separate modified gamma distribution to each mode.

As there is infinity of fog in the nature, there is an infinity of DSD to characterize them. Some authors have proposed to define some parameterisations for different "families" of fog: "Maritime fog" and "Continental fog".

- "Maritime fog" is usually composed with big droplets (> 5 -10 µm). It could be considered as representative of advection fog (see definition of fog types in 3.1.2 - Fog formation)
- "Continental fog" is composed mostly of small droplets (few µm). It could be considered as representative of radiation fog (see definition of fog types in 3.1.2 - Fog formation).

Figure 3.7, below shows some parameterisation that are considered in Muhammad et al. (2007). This figure gives also some parameterisation for some cumulus clouds.

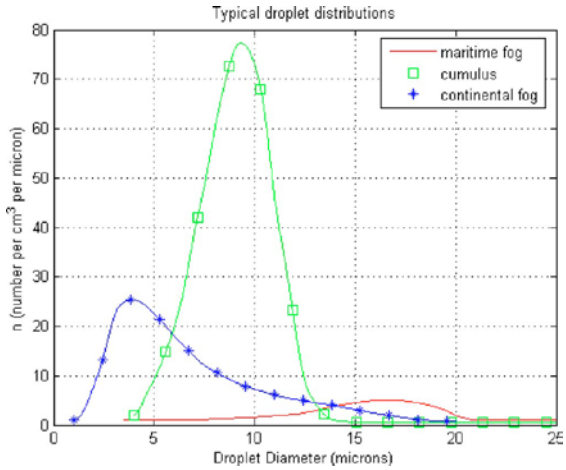

Figure 3.7: Typical droplet distribution for different kinds of fog. From Muhammad et al. (2007).

<u>Relating visibility to the size distribution:</u>

In the visible part of the spectrum, the droplets are efficient at scattering the radiation, while they only weakly absorb. The extinction efficiency (Q_{ext}) of a droplet is defined as the amount of radiation it scatters or absorbs relative to the radiation that passes its cross section area ($\pi D^2/4$). Thus, the extinction coefficient is (I Gultepe, Müller, & Boybeyi, 2006):

$$\beta = \int_{D_{min}}^{\infty} \frac{\pi}{4} Q_{ext}(D)\, n(D) D^2 dD$$

Unless the droplet is very much bigger than the radiation wavelength, the scattering cross section is a function of the size of the droplet relative to the wavelength (Liou, 2002). For visible radiation (wavelength < 700 nm), droplets are so much bigger (2 to 10 times the value of the wavelength) that extinction efficiency is almost constant and equal to 2, so that the visible extinction coefficient is well approximated by (Hu & Stamnes, 1993):

$$\beta = \frac{3\, LWC}{\varrho_w\, D_{eff}}$$

Combining this with Koschmieder's equation (see section 3.2), we get

$$Vis = \frac{\varrho_w D_{eff}}{LWC}$$

So the visibility decreases with LWC, but it increases with the droplet effective radius. This means that for the same liquid water content, the extinction will be larger and the visibility lower if the water is spread across more and smaller droplets (see examples in Table 3.3). The number of droplets is closely related to the number of CCN in the air-mass, as explained above.

Table 3.3: Examples of visibility calculated from LWC and effective diameter (see equation in the text).

Liquid water content (LWC), g/m³	***Effective diameter (D_{eff}), µm***	**Water density (ϱ_w), g/m³**	***Visibility (m)***
0.1	10	10^6	100
0.1	30	10^6	300
0.01	5	10^6	500

Fog interaction with infrared radiation

Terrestrial objects emit IR radiation, and technologies exist which can use this radiation to see obstacles; e.g. Beier and Gemperlein (2004) describe such a system in use for airplanes. Fog droplets scatter, absorb and emit IR-radiation and will therefore distort images based on IR as well. Droplets are not much bigger than the wavelength of IR, so that the scattering efficiency can vary much more with size; generally, bigger droplets have a larger scattering efficiency than smaller droplets (Liou, 2002, p. 191). According to Hu and Stamnes (1993) the extinction is proportional to LWC, and it is also dependent of the wavelength, mostly for the smallest droplets of effective diameter of 6 µm (Figure 3.8).

An interesting question is whether the "visibility" in IR is better than the visibility in the visible spectrum (corresponding to the extinction in IR being smaller than the extinction in the visible). Beier and Gemperlein (2004) state that for particles of size smaller than 1 µm (haze), the visibility is much better in IR than in the visible, while the visibility is equally bad in IR as in the visible when droplets grow larger than about 5-10 µm. From the results of Hu and Stamnes (1993) shown in Figure 3.8, it can also be seen that a population of relatively large droplets (effective radius of 6 µm, i.e. D_{eff} = 12 µm) has significantly lower extinction for wavelengths ~10 µm and >20 µm than in the visible (0.3-0.7 µm). However, when the effective radius is even larger (15 and 24 µm radius in the figure), the improvement in visibility occurs for wavelengths larger than 100 µm. In summary, the IR is more useful for seeing through fog with smaller droplets than fog with larger droplets. The effect of the wavelength on radiations attenuation will be developed both for fog and rain particles in 4.1.4 - Impact of the wavelength.

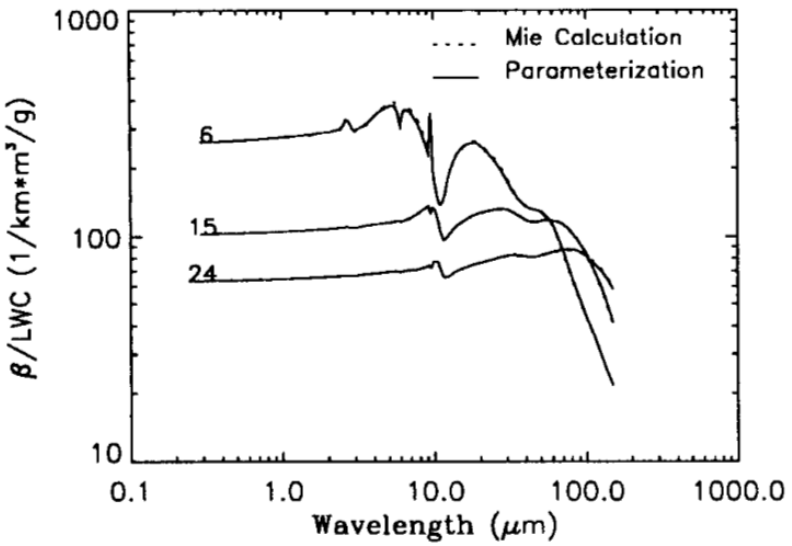

Figure 3.8 : The extinction coefficient of a DSD per LWC as function of radiation wavelength for three different effective radii (Mie calculations and a parameterisation based on LWC and Deff give almost identical results). From Hu and Stamnes (1993).

<u>Summary: Theory of fog microphysics</u>

The droplet size distribution (DSD) is used to describe how many droplets are present in different size bins. The droplets are distinguished from smaller, unactivated haze particles by having passed a critical size (about 1-3 µm diameter), which allows them to grow spontaneously. The total number concentration of droplets in the fog is strongly dependent on the number and types of aerosols in the air-mass where the fog forms; more and smaller droplets are formed if the air-mass contains a larger number of soluble aerosols (due to e.g. pollution). The visibility depends on the liquid water content (LWC) and the droplet sizes (through the effective diameter); if the droplets are smaller and more numerous with the same LWC, the visibility will be less (due to larger surface area). The haze particles can also contribute significantly to reducing the visibility, but in fog the droplets contribute to most of the reduction in visibility. The fog is more transparent in the infrared spectrum than in the visible when the droplets are small, while for larger droplets there is not much difference.

3.3.2 Experimental studies of fog microphysics

Several experimental studies of the microphysics in fog have been performed at various locations with different air masses. In the following, fog microphysical properties from a few more recent studies will be presented. Some key numbers found in these studies are presented in Table 3.4.

Price (2011) studied fog cases in Cardington (England) by measuring DSD at 2 m with a cloud-droplet probe (CDP). He found an increase in droplet sizes from formation phase to mature phase. Initially droplets were of diameter ≤10 µm. After 3-4 hours, bigger droplets appeared so that the mean diameter increased to around 15-20 µm, and the droplet distribution became much wider (Figure 3.9). Such a transition from a domination of smaller droplets to the appearance of larger droplets during the early phase of a radiation

fog event was also found by Degefie et al. (2015) based on fog measurements near Paris (France). However, Degefie et al. (2015) also studied a stratus-lowering fog event, and it did not show such a transition, which is not so surprising as such a fog forms from an already well developed cloud. In both cases, droplets of diameter 25-30 µm contributed importantly to the liquid water of the mature fog. Degefie et al. (2015) also studied the vertical motion of droplets and concluded that there are smaller droplets rising, while the larger droplets are falling. Although fewer, these larger droplets contain more liquid water.

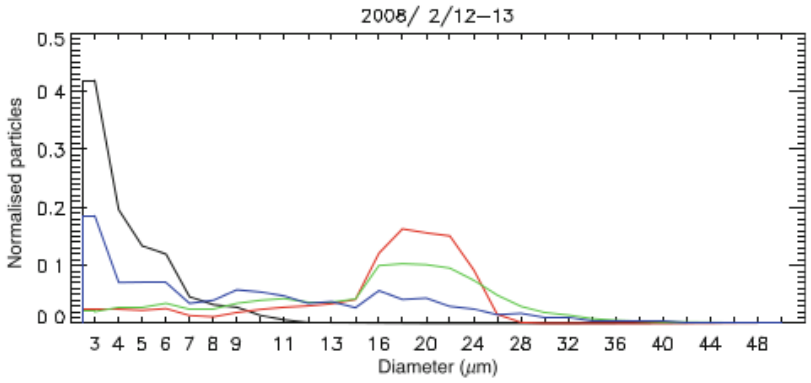

Figure 3.9: Droplet size at different times during a fog 12.-13. February 2008 in Cardington (England). 18:50-21:00 UTC (black), 22:00-24:00 UTC (red), 06:50-09:00 UTC (green), 11:30-12:40 UTC (blue). From Price (2011).

The Paris Fog project (J. Dupont, Haeffelin, Stolaki, & Elias, 2016; Haeffelin et al., 2010), operating since 2006 in the Paris region, aims to explore fog processes and therefore can provide detailed ground-based observations of fog events in this area (~30 fog events per winter season), in particular from the SIRTA atmospheric observatory. Mazoyer (2016) studied 42 fog cases during 3 winters (2010-13) at SIRTA. The DSD was measured using the fog monitor FM-100 instrument, which measures sizes 2-50 µm. The median value over all fog for LWC was 0.024 g/m^3, effective diameter 14 µm, and droplet concentration 61 cm^{-3}. These quantities varied significantly, as presented in Table 3.4. Figure 3.10 shows the average DSD for 4 of the fog cases studied by Mazoyer (2016). It illustrates that the DSD can vary much from one fog to another; it can have one or several modes, and there may be significant amounts of droplets up to 50 µm diameter in some cases, while in other cases the droplets are all smaller than 15 µm. Mazoyer (2016) also notes that there is no clear separating dip in the size distribution between inactivated aerosols and droplets, as previously mentioned. Mazoyer (2016) also found that the droplet number concentration is largely determined during the formation of the fog; during the fog life cycle the droplet sizes change while the number of droplets remains quite unchanged.

Statistics of the microphysical properties from the Paris Fog dataset is also presented by Burnet et al. (2012). In Figure 3.11 they present statistics of microphysical properties during 21 of the fog events (they used a smaller part of the dataset than Mazoyer (2016)). The LWC is dominated by small values, it is nearly always less than 0.1 g/m^3 with a median of 0.038 g/m^3. The droplet number concentration varies from less than 10 cm^{-3} to 200 cm^{-3}, with a median of 75 cm^{-3}. The effective diameter ranges 5-25 µm, most frequently it is 10-15 µm.

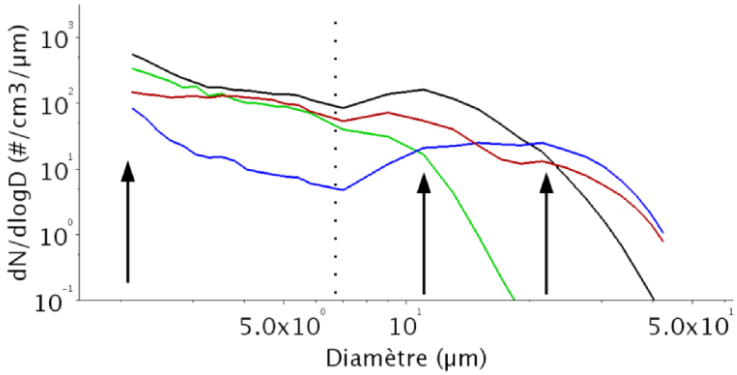

Figure 3.10: Average size distributions during 4 different fog events observed at SIRTA (Paris). Note that both axes are logarithmic. From Mazoyer (2016).

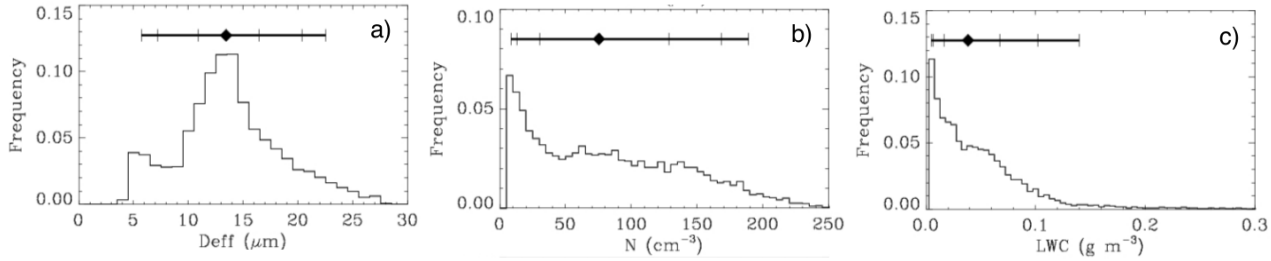

Figure 3.11: Frequency distribution of different values of (a) effective diameter, (b) droplet number concentration and (c) LWC, during 21 fog events in 2010-11 at the SIRTA observatory near Paris. The diamond marks the median, and the ticks mark percentiles 5, 10, 25, 75, 90 and 95. From Burnet et al. (2012).

Gultepe et al. (2009) studied fog in south eastern Canada at one continental (Egbert, Ontario) and one coastal (Lunenburg, Nova Scotia) site. The DSD during fog was measured with a fog monitor. At both locations, the median value for LWC was around 0.02-0.03 g/m^3. The droplet number concentrations were slightly higher on the coastal site than the continental site (median value of 90 cm^{-3} v.s. 50 cm^{-3}). The sizes were smaller than in the ParisFog studies, with a median effective diameter of 8 µm at both locations.

Table 3.4: Fog microphysical statistics from some recent observational studies. The results from Price (2011) are typical values among 7 fog events, the results from Mazoyer (2016) are 25-75 percentile values from 42 fog events, and the numbers from Gultepe et al. (2009) are the median and 10-90 percentiles of their measurements.

Location	Comment	LWC (g/m^3)	Number conc. (cm^{-3})	Modal diameter (µm)	Effective diameter (µm)	Reference
Cardington (England)	Early phase			3-4		Price (2011)
Cardington (England)	Mature phase			16-18		Price (2011)

Suburban Paris (France)	All phases	0.005-0.075	19-164	8-19	Mazoyer (2016) (incl. Burnet et al., 2012; Degefie et al. , 2015)
Egbert (Canada)	Continental fog	0.03 (0.02-0.2)	50 (25-100)	8 (5-12)	Gultepe et al. (2009)
Nova Scotia (Canada)	Marine fog	0.03 (0.02-0.1)	90 (50-170)	8 (4-13)	Gultepe et al. (2009)

Finally, it is worth noting that the microphysical properties may change on the vertical. As most observations of fog microphysics are done near the surface, the vertical profile is not well known. Cermak and Bendix (2011) discuss the vertical profile of LWC in fog, developing a theoretical shape of the profile; notably the LWC is expected to increase with height throughout most of the fog, due to adiabatic vertical motions and heat conduction from the surface, but decrease with height near the top due to dry air entrainment. Egli et al. (2015) observed the vertical profiles of LWC in two fog events with a cloud droplet probe (CDP) attach below a tethered balloon deployed in Linden, Germany. They found largely good agreement with the profiles of Cermak and Bendix (2011) during the mature phase of fog (LWC increasing with height). During dissipation phase, the LWC was found to be highest near the surface, which they interpret to be due to evaporation of the fog from above and the settling towards the ground of bigger droplets.

Summary: Observational studies of fog microphysics

Observational studies of fog microphysics indicate that the DSD can vary much from one fog case to another. In some cases, the fog is dominated by small droplets (diameter below 10 µm), while in other cases significant amounts of droplets with sizes well above 20 µm are present. The sizes of the droplets can also change during one fog event; in radiation fog small droplets often dominate in the early phase, while larger droplets appear later. The DSD is observed to have one mode in some cases, while in others it may have two modes, one for the smaller, more numerous droplets and one for the bigger droplets, which will typically contain more liquid water. The LWC in fog is often below 0.1 g/m^3, but larger values of 0.1-0.5 g/m^3 can also occur.

3.4 Fog observation techniques

3.4.1 Visibility measuring instruments

There are different approaches for measuring visibility. While some techniques estimate the atmospheric extinction coefficient and apply Koschmieder's equation, others mimic the eye vision by using photographic techniques to view a target (Tombach & Allard, 1980). In the following a short presentation of these different approaches is given.

Measurement techniques using atmospheric extinction:

To estimate the atmospheric extinction coefficient, there are two main approaches, transmissometers and diffusiometers. The theories of these instruments are briefly introduced below, based on the description of

Holejko and Nowak (1997) unless otherwise stated. Both instruments emit a laser beam, which passes through a volume of air before being detected by a receiver.

In a *transmissometer*, the emitter and receiver are aligned, so that the extinction of the beam can be measured directly from the difference between the emitted and received power (Figure 3.12). The drawback of this approach is that the receiver and emitter must be placed at a significant distance from each other for this difference to be sufficiently large to get a precise measurement of the extinction, which makes it less applicable to mobile use.

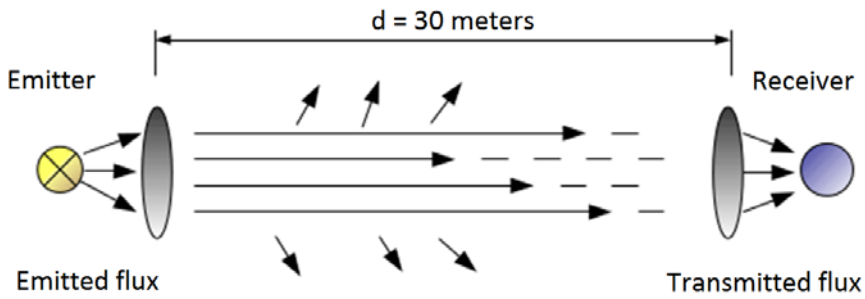

Figure 3.12: Schematic of the principle of a transmissometer. From Babari (2012).

Diffusiometers use the scattered light in a specific direction to estimate the extinction. In this case the transmitter and receiver are not aligned, so that the receiver measures how much light is scattered in an angular interval, which is the intersection between the transmitted beam and the field of view of the receiver (see Figure 3.13). Usually the angle is less than 90 degrees, and then the instrument can also be called a *forward scattering visibility meter*; an example is the DF20, which is displayed in Figure 3.15 and described in Table 3.5. To relate the scattering in this specific direction to the atmospheric extinction, assumptions have to be made on the single scattering albedo (relative importance of absorption and scattering) and phase function (how the scattering is distributed in the different directions) (Liou, 2002) of the scattering particles. These properties differ between various atmospheric compounds, illustrated by the phase functions in Figure 3.13. As fog droplets are the most important particles for reducing the visibility, their properties are assumed when calculating the extinction coefficient, and a correction is needed for a precise visibility estimate in the case of other particles (Elias et al., 2015). A measurement of visibility from a diffusiometer therefore has an inherent uncertainty due to these assumptions on the optical properties of the particles. Forward scattering visibility meters using several detectors located at different angles have also been developed; these are able to detect the type of scattering particle (fog, mist, haze) and give an improved measurement of visibility (Li & Peng, 2012). The AMS glossary calls such diffusiometers using several angles *nephelometers* (Glickman & Zenk, 2000). Crosby (2003) discusses the accuracy in measurements by forward scattering visibility sensors. He presents several available instruments and argues that an accuracy of 10-20 % is achievable.

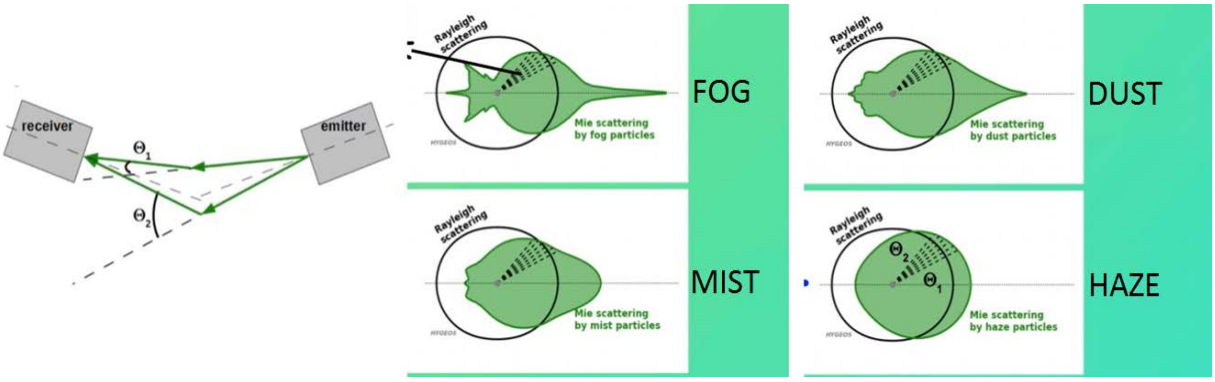

Figure 3.13: Illustration of the functioning of a forward scattering visibility meter (left), and schematic of the phase functions of various types of scattering particles (fog, mist, desert dust and haze (right). From Elias et al. (2015).

Present weather indicators are instruments that detect various aspect of the present weather, such as precipitation, cloudiness and visibility (Wong, 2012). The PWD22 is one such instrument, which can be used as a visibility meter as well as detect the amount and type (liquid versus solid) of precipitation (Guyot et al., 2015).

Since ice crystals do not scatter the light in the same way as droplets, diffusiometers may be less accurate in ice fog conditions. In their review on ice fog, Gultepe et al. (2015) mention that the present weather detector FD12P (Vaisala Inc.) and the diffusiometer "Sentry visibility sensor" (Enviroteh Inc.) have been used for measuring the visibility in ice fog.

Measurement techniques using cameras:

For the visibility measurement on the road, recent studies (e.g. Babari, 2012; Hautiere et al., 2006) suggest to use cameras to estimate the visibility distance from on board moving vehicles. An obvious advantage of a camera image relative to using the measurement of atmospheric extinction is that the image can give a more direct representation of what the driver of the vehicle actually can see, which not only depends on atmospheric extinction, but also on the contrast of the objects existing in his field of view (as discussed in section 3.2). However, camera techniques require robust image processing methods in order to give a reliable visibility estimate, and this is a major focus of the above mentioned studies.

For example, Hautière et al. (2006) describe a photographic technique for measuring the visibility from a vehicle on the road in real time. They use a camera whose images are analysed to detect the furthest object with a contrast above the 5 % threshold (i.e. the mobilized visibility defined in section 3.2). Some examples of their results are shown in Figure 3.14. We see that in case (a) the mobilized visibility is limited by the curvature of the road, while in cases (b-c) it is limited by the fog.

The camera approach has also been studied for stationary use. A recently developed photographic instrument for measuring visibility is presented by Wang et al. (2014). They found that this instrument agreed better with human visibility than a forward scattering visibility meter and provided more stable and accurate visibility measurements both during rainy and foggy conditions.

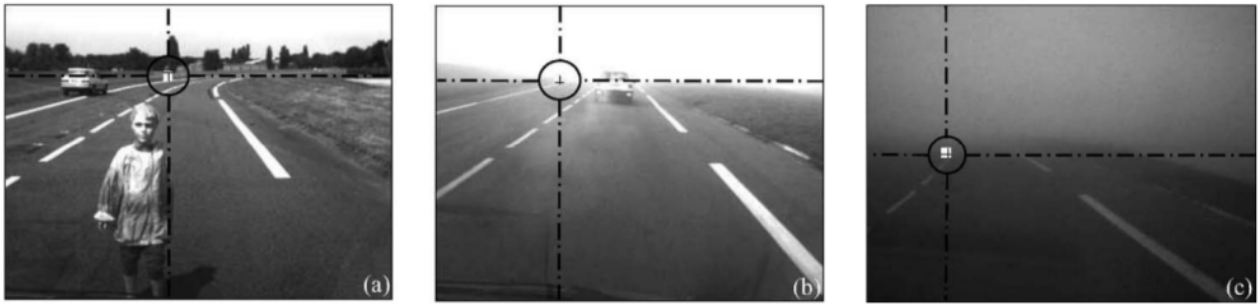

Figure 3.14: Results from a detection method for the mobilized visibility (V_{mob}) by contrast in camera images: (a) sunny conditions ($V_{mob} \approx 250$ m), (b) fog ($V_{mob} \approx 75$ m), and (c) dense fog ($V_{mob} \approx 30$ m). The most distant visible object on the road is indicated. From Hautière et al. (2006).

Summary: Visibility measuring instruments

The *meteorological* visibility can be measured either by a transmissometer, which requires sufficient distance between transmitter and receiver, or by a diffusiometer, which has uncertainties due to the assumptions on the properties of the scattering particles. A very different approach for visibility measurement is to use camera images. This latter approach can be specifically developed for a use on the road. However, since several factors apart from the atmospheric extinction affect it (background light, road curvature, presence of contrasted objects), the visibility calculated from this approach will not have a direct relation to the fog physical properties.

3.4.2 Instruments measuring microphysical characteristics

Microphysical properties of fog can be measured in-situ by sensors that are in direct contact with the air containing the droplets. This section will first introduce how these sensors work and give examples of existing instruments, then present the various uncertainty sources, and finally present some reflections on the possible usage on a vehicle.

Technical principles and examples:

The principles of instruments that measure cloud microphysics in-situ are described by Guyot et al., (2015). There are two main types. Firstly, *single particle counters (SPC)* are instruments that size and count individual droplets, and they can therefore directly measure the DSD. These instruments let the air containing the droplets flow past a thin laser beam. When a droplet passes the laser, the beam is scattered, and a receiver measures the energy diffused in a certain angle (typically in 4-12˚), and this is used to estimate the size of the droplet. The laser should be sufficiently thin so that only one droplet passes the sampling volume at a time. The airflow past the laser can be maintained by a pump; however, if the instrument is meant to be carried by an aircraft, the air will flow into the instrument by itself; in that case the speed of the airflow must be measured. Instruments that are meant for aircraft use and therefore don't have a pump can still be supplied with one if they are to be used on the ground, as was done for the FSSP by Guyot et al. (2015).

The second type of instruments, *ensemble-of-particle probes (EPP)*, uses the scattering by an ensemble of droplets passing through a much larger sample volume to estimate bulk-average quantities such as the LWC and total droplet surface area, but without providing a DSD. Several of the instruments mentioned in the previous section (diffusiometers, transmissometer) can therefore also be considered EPPs, since they measure the ensemble quantity *visibility*. EPPs don't need airflow, since they measure the whole droplet population at once.

In the following, we give a short presentation of 6 SPC instruments and 1 EPP instrument. A summary of their measurements, time resolution and size is given in Table 3.5, and photos of the instruments in Figure 3.15.

- The Forward scattering spectrometer probe (FSSP) is the oldest SPC still in use for measuring the DSD; it can measure droplets in the range 2-47 µm with 15 channels (Guyot et al., 2015). An evaluation of its functioning and important precision issues is discussed in Dye and Baumgardner (1984). Brenguier et al. (1998) describe an improved version, the Fast FSSP (SSP-100), showing that several sources of uncertainty in the measurements have been reduced relative to the FSSP.
- The cloud droplet probe (CDP) measures the size range 3-50 µm. Its performance has been studied in laboratory and aircraft campaigns (Lance, Brock, Rogers, & Gordon, 2010).
- The Fog monitor (FM-100) is a forward scattering spectrometer probe (λ = 0.658 µm) placed in active ventilation (pump) (Eugster, Burkard, Holwerda, Scatena, & Bruijnzeel, 2006), manufactured by Droplet Measurement Technologies, Inc., Boulder, USA and designed for ground-based measurements. This instrument measures droplets in the size range 1.5-50 µm, using 10-40 channels which can be defined by the user (Spiegel et al., 2012). A newer version of this instrument is the FM-120.
- PALAS WELAS-2000 can detect particle sizes in the range 0.39-42 µm in 65 bins (Elias et al., 2009). Elias et al. (2009) showed that the WELAS did not efficiently enough sample the bigger fog droplets (>10 µm); this was also found by Burnet et al. (2012). Conversely, the FM-100 was found to under-estimate the concentrations of the smallest droplets (<~6 µm). These two instruments can therefore complement each other (Elias et al., 2015).
- The light optical aerosol counter (LOAC) (Renard et al., 2016) is a newly developed instrument. As the fog monitor, it has an active pumping system. It has the advantage of being small enough to be lifted by a tether balloon and thus measure DSD at higher altitudes. It can measure the diameter range 0.2-100µm (aerosols and droplets) with 19 channels (NB: 40-100µm is represented by only one channel). Renard et al. (2016) performed a comparison between the instruments LOAC, WELAS and a fog monitor during a fog event (Figure 3.16). It can be seen that the LOAC agrees relatively well with the other two instruments within their respective size domains of precise measurement mentioned above.
- The particle volume monitor (PVM), which is an EPP, has two sensors, one measuring the total volume of the cloud droplets and the other the total surface area (Gerber, Arends, & Ackerman, 1994), thus allowing estimations of LWC and D_{eff}. The PVM measures the laser light (at λ = 0.780 µm) scattered in the forward direction by an ensemble of cloud droplets which crosses the probe's sampling volume of 3 cm³ (length of 42 cm by sampling area of 7 mm²). The light scattered in the 0.32-3.58° angle range is collected by a system of lenses and directed through two spatial filters. More detailed description of

PVM-100 (ground-based) can be found in Gerber (1991), while a description of the airborne version PVM-100A in given in Gerber et al. (1994).

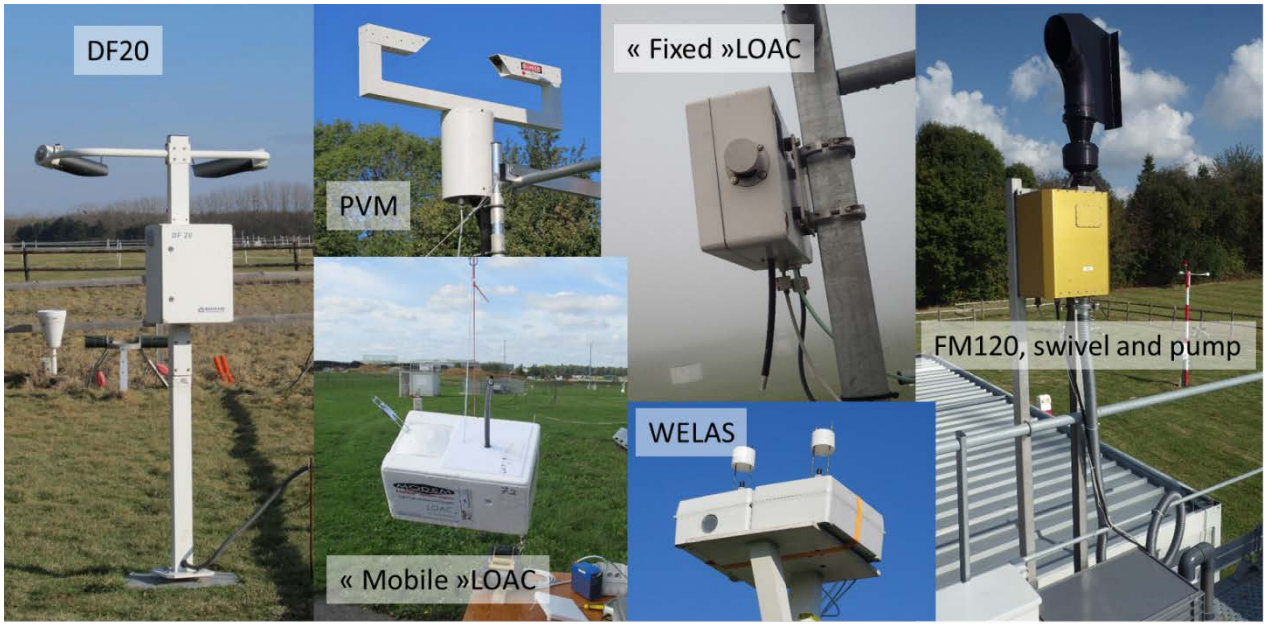

Figure 3.15: Photos of several instruments measuring properties of fog droplets (see Table 3.5 for details). Copyright SIRTA.

Table 3.5: Key parameters of instruments measuring properties of fog droplets (Elias et al., 2015; Guyot et al., 2015).

Instruments	Measured parameter	Measurement range (diam.)	Time resolution	Pump for air inlet?	Size / weight
Diffusiometer (DF20, DF320, PWD)	Extinction (visibility)	All	1min	no	H 3-4m x L 1m x l 1m x W 50kg
PVM	Extinction, LWC and effective diameter	3-45µm	5min	no	H 0.5m x L 0.7m x l 0.2m x W 5kg
FM100-FM120	Size distribution	2-50µm	1sec	yes	H 1m x L 1m x l 1m x W 30kg
LOAC	Size distribution	0.2-100µm	10sec	yes	H 0.2m x L 0.2m x l 0.2m x W 2kg or 0.6kg
WELAS	Size distribution	0.4-10µm	1sec	yes	H 0.2m x L 0.2m x l 0.2m x W 2kg
FSSP	Size distribution	2-47µm	1sec	no	H 0.2m x L 0.4m x l 0.2m x W 15kg
CDP	Size distribution	2-50µm	1sec	no	H 0.2m x L 0.2m x l 0.2m x W 2kg

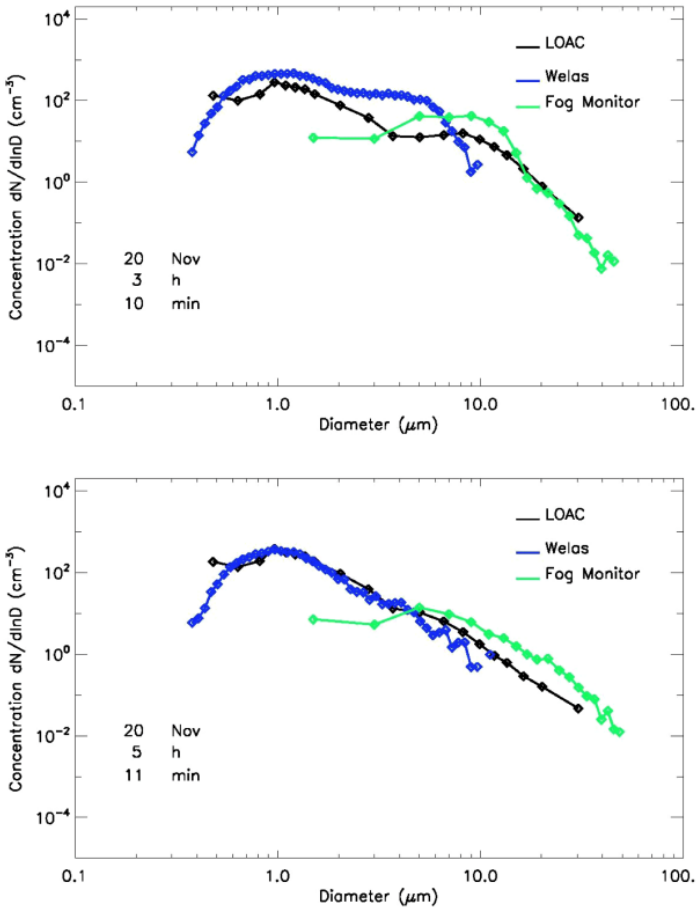

Figure 3.16: Comparison of three SPC instruments during a fog event 20. November 2012 in the ParisFog field campaign. Top: At beginning of fog. Bottom: At the end of the fog. From Renard et al. (2016).

Measuring the microphysics from a vehicle

Of interest to the DENSE project is the possibility to measure the DSD of fog from a vehicle in motion. Apart from obvious limitations in the size and cost of the instruments, a reliable measurement would require a known, stable airflow and an accompanying bulk measurement:

- **Air flow:** As mentioned before, a continuous and known air-flow is needed in order to measure the DSD with an SPC. When the vehicle is in motion, the same principle as an aircraft could be applied, that is letting the air enter the instrument by itself. The airflow through the instrument would need to be measured, though, as it would vary due to variations in the wind speed and in the speed of the vehicle. A 2D sonic anemometer could be installed on the roof of the vehicle to precisely measure air velocity compared to the SPC. If the vehicle stops or moves slowly (~<30 km/h), the airflow through the instrument might not be sufficient. To be able to measure also in these cases, a pumping system should then be switched on to ensure an airflow around 10-15 m/s inside de SPC. The usage of the pump at higher speed is discouraged, since it might cause turbulence which would disturb the measurements.

- **Bulk measurement:** As already mentioned above, the DSD measured from an SPC needs to be normalized by a bulk measurement. We suggest using the visibility measured by a diffusiometer for this, as the visibility would also be of direct interest.

Thus, a possible set-up for measuring the size distribution from a vehicle would be an SPC, for example the FSSP, accompanied by a diffusiometer for normalisation. The SPC must be provided with a wind speed measurement at its inlet. If it should measure also when the vehicle is stopped, it must also have a pump.

Summary: Instruments measuring microphysical properties

The measurement of the droplet size distribution in fog is carried out using single particle counters (SPCs), which count and size the droplets using a laser. This technique involves several uncertainty sources, in particular when the wind direction is not parallel to the air inlet. These instruments can typically measure droplets up to 50 µm of diameter, but some of them will underestimate the presence of the big droplets (10-50 µm). Since SPCs are not calibrated in number, their size spectra must be normalized using an ensemble property measurement (e.g. visibility, LWC). In order to give correct measurements, an SPC needs a stable and known airflow passing through it. This airflow is provided by a pump for stationary instruments, while for aircraft based instruments it is provided by the airplane's motion. To measure from a vehicle in motion on the road, a passive air inlet as that on an aircraft-based instrument could be used; however, a pump would need to be used if the car slowed down too much or stopped.

4 Rain

4.1 Rain and perception

4.1.1 Impact on human perception

Rain affects perception of the road environment in different ways. Like fog, heavy rain can reduce transmission through the atmosphere, by scattering light. But it also has other effects: the impact of water on the windscreen, water sprayed up from the road by vehicles, light reflected from wet objects, etc. (Hautière, Bigorgne, & Aubert, 2008).

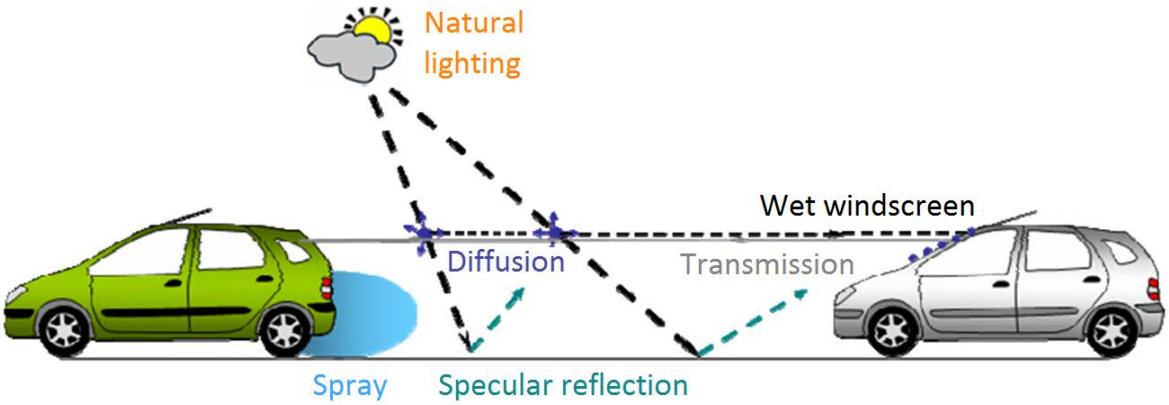

Figure 4.1: Effect of rain on driving. From Hautière et al. (2008).

Rain directly affects the driver's perception (transmission through the atmosphere) but also produces changes in visibility through its action on vehicle headlights and windscreens. It also reduces the visual effectiveness of road markings and their contrast with the road by day and by night.

An object lit by the sun, street lighting or vehicle headlights, is perceived by the light it reflects. Rain interferes with this process in several ways:

- Rain makes headlights and other light sources less efficient by filtering out some of the flux and reduces road lighting ahead of the vehicle, like the reflected portion.
- Part of the light is scattered backwards towards the driver. Backscatter acts as a veil that reduces the contrast of objects within the driver's field of view. It thereby reduces the driver's detection ability.
- Low visibility complicates the driver's task. As a result, he is less focused on his peripheral vision, which can make it more difficult to detect a vehicle or pedestrian approaching from the side.
- It affects the driver's ability to see through the windscreen. Even with the windscreen wipers running, splashing water and the wipers themselves periodically reduce vision.
- It also affects visibility of markings and pedestrian crossings that are covered with a film of water and are no longer retroreflective. Ultimately, the markings become virtually invisible to the driver.

- The road is therefore darker than in dry weather. Because its surface acts as a mirror, other light sources are reflected from the road and may create visual discomfort or glare.

Studies of these effects under actual driving conditions are difficult to conduct, for reasons of safety and also because they cannot guarantee reproducibility. This is why more in-depth studies are usually performed in more controlled conditions, on test tracks or platforms.

Ivey, Lehtipuu, & Button (1975), conducted a driver visibility study on a test track. For this, a camera is used on board a vehicle set in motion under rain booms. Visibility is estimated by the contrast between an object to be detected and the background of the scene. Driver visibility loss is therefore related to three parameters: rainfall rate, vehicle speed, and windscreen wiper frequency (Ivey et al., 1975).

Bernardin et al. (2014) studied visibility loss in rain in the laboratory on contrast threshold detection spots, and readability loss on characters on a simulated signboard for two rainfall rates and two types of wipers (Bernardin et al., 2014).

All these identified effects that disrupt driver perception also have effects on computer vision systems, regardless of their technology.

4.1.2 Analysis at raindrop level

In order to understand these phenomena, Baker & Nayar (2003) proposed a model of the interaction of light with a raindrop. It breaks up the luminance emitted by the drop in a given direction as a function of the reflected luminance from the outside, the refracted luminance and luminance from internal reflection. In this way, a raindrop can be modelled as a lens that reflects and refracts light from the environment to the observer. This model leads to the conclusion that a raindrop emits light perceived behind it in a 165°cone.

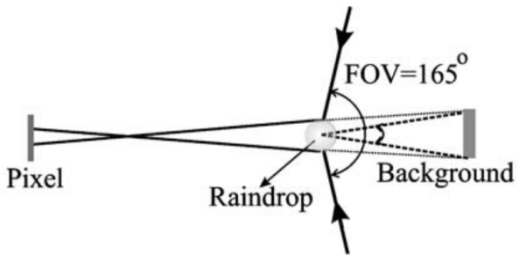

Figure 4.2: Field of view of a raindrop. From Garg & Nayar (2007).

For outdoor scenes in broad daylight, considering that the sky predominates in the 165° cone, it may be considered that raindrops emit a constant luminance (denoted L), generally greater than that of the scene (Garg & Nayar, 2007). By night, more complex modelling taking into account each light source is required (Garg & Nayar, 2006).

4.1.3 Impact on computer vision systems

Concerning computer vision, rain produces an image flicker and may hide objects in the scene. It therefore reduces the effectiveness of computer vision systems (Tripathi & Mukhopadhyay, 2011). This may be the

case, for example, in an object tracking algorithm (P. C. Barnum, Narasimhan, & Kanade, 2010). In general, free-falling raindrops particularly degrade computer vision systems that use descriptors with high spatial frequency components: object tracking, stereo image matching, object recognition, segmentation, edge detection, or noise suppression (Kumar & Sudipta, 2012). It is therefore particularly important to take the impact of rain on the images into account. Yet although some research on computer vision systems for roads takes into account degraded weather conditions (Shehata et al., 2008; Siogkas & Dermatas, 2006), most use only images acquired in favourable conditions.

Shehata et al. (2008) offers a bibliographic review of elements that may pose problems for automatic incident detection systems (AID). Static shadows caused by the environment on roads, snow on roads, rain causing reflections (water on the road) and reflections on roads are the main causes of false alarms. The false alarm rate is currently high for these systems: from 60% to 80% as compared with all alarms, and weather conditions are the main cause of this. However, if there are too many false alarms, the operator will prefer to stop the automatic system rather than to use it. Conversely, illumination problems or fog may cause missed detections, which is equally problematic. One solution to avoid most false detections related to adverse weather conditions is to use stereoscopic cameras (Shehata et al., 2008). Visual effects from shadows, snow, or reflections are eliminated by the absence of an object (these purely visual effects are of height zero). Stereoscopic cameras are however not yet in the majority.

4.1.4 Impact of the wavelength

Computer vision systems, visible light cameras, infra-red, laser scanner and radar, are based on technologies using various electromagnetic radiation. These radiations may be affected differently by the atmosphere including rain and fog. Al Naboulsi (2005) examined telecommunication technology using atmospheric optical transmission. As with driver assistance systems, the atmosphere disturbs signal transmission and information. Based on the work of Klein (1997), he shows the effects of the atmosphere on the transmission of electromagnetic waves. On Figure 19, the thick oscillating line gives the absorptions of certain constituents of the atmosphere (H_2O, CO_2, O_2 ...).

The signal attenuation versus wavelength depends both on:

- the concentration of the droplet, that means: fog density, rain intensity that is related to the liquid water content, LWC
- and the particles size, that is in the following range: microscopic particles ranging about from 0,4 to 40 µm, for fog and 0.05 to several millimetres for rain.

Then Figure 4.3 shows a significant signal attenuation, with dense fog (LWC = 0.1 g/m3) on the top right of the figure, that is in abscise for the wavelengths of visible and infra-red light. While heaviest and heavy rain (high concentration of particles of 0.1 to several millimetres) may affects, more than fog, millimetre and sub-millimetre waves (radar range of wavelength). This contributes to understand why when using only one sensor with some specific radiation band, this doesn't allow to detect all the objects of the road environment in all weather conditions. This is the challenge of the DENSE project to find a sensors suite that mixes the technologies, and with adapted data fusion, reach the goal of the all-weather systems.

In driving conditions, some technologies are more adapted for road guidance, some others for pedestrian detection at night, and some others for vehicle detection. The task of this ADAS, is to provide some automatic guidance (by lane detection, detection of road markings or road sides), but also some target detection (for collision avoidance). Indeed, target detection depends on: the signal transmission, the apparent size of the target and the properties of emission or reflection of the target and the contrast between the target and the background around the target.

Figure 4.3 gives only information's about the signal attenuation (measured between an emitter and a receiver), then other parameters have to be considered:

- The apparent size of the target that you consider is linked to the distance. In fact, you need to detect the target enough time in advance (at a sufficient distance) for the driver reaction or for the car automatic breaking. This induces that the system must detect the obstacle at a long distance, when its apparent size is rather small. This has to be taken into account in the requirements of the angular resolution of the sensors of the DENSE system.
- The properties of emission or reflection of the target need to be considered for the various wavelength of the sensors suite. Then before the experimentation, a survey is required on existing data base about emission or reflection of natural road target in all wavelength, and also on "artificial" calibrated targets.

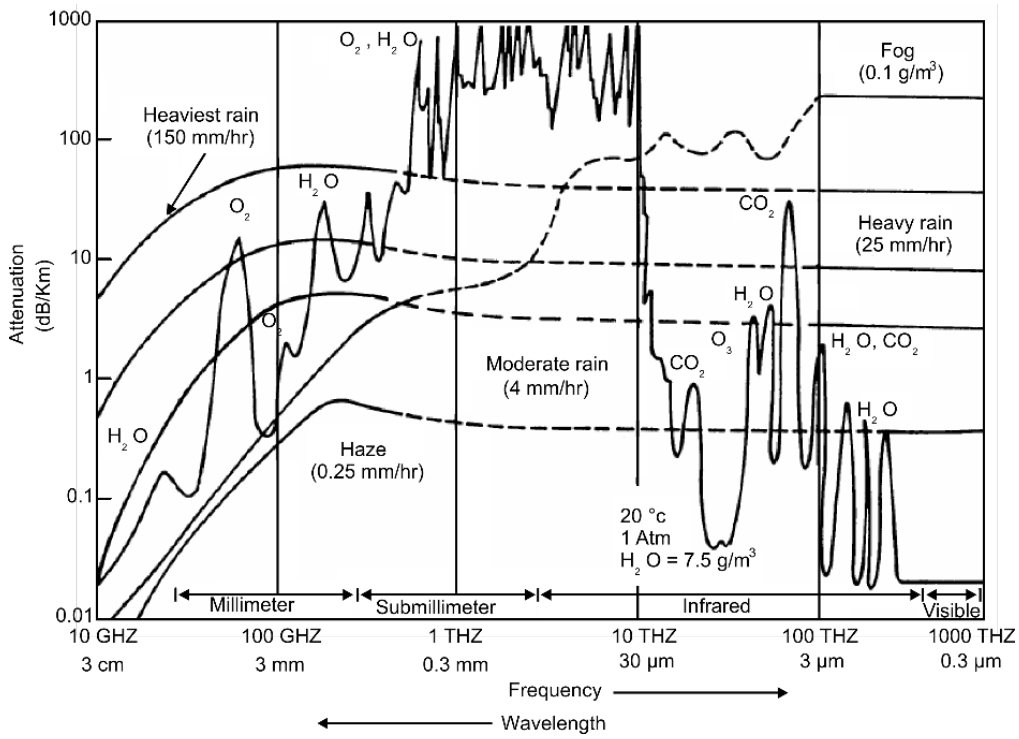

Figure 4.3: Atmospheric attenuation spectrum (dB/km) from 0, 3 microns to 3 cm, showing the effect of certain constituents of the atmosphere on attenuation and that of rain and fog (. Al Naboulsi (2005) and Klein (1997).

4.1.5 Loss of visibility by transmission of the atmosphere

By analogy to fog, heavy rain may be considered as a scattering medium consisting of water droplets which fall to the ground with a certain velocity. The effect of the water droplets is to absorb and/or scatter light passing through them.

The absorption and scattering phenomenon therefore causes attenuation of the light intensity of a light beam passing through the rain curtain with distance, according to the following relationship:

$$I(d) = I_0 e^{-k_p.d}$$

where I_0 is the light intensity of the light beam at the entrance to the rain curtain, d is the length of the rain curtain in m, k_p is the extinction coefficient in m-1 and $I(d)$ the light intensity of the light beam at the exit from the rain curtain.

4.1.6 Loss of visibility by reflection on the road surface

Road surfaces have optical reflection properties which depend mainly on the kind of materials that compose them, and on their roughness. Rain partially or entirely covers road surfaces with a film of water which runs away more or less quickly with the slope of the road.

This new interface modifies the reflective properties linked to the presence of a water film on the surface and/or to the infiltration of water into the surface depending on the porosity of the material.

Loss of visibility is particularly critical when road markings start to become covered with a water film. Marker strips are the main guiding feature to help the driver keep his vehicle in its lane by day and especially by night.

Similarly, driver assistance systems that ensure the same function of automatic vehicle guidance rely on computer vision systems that detect marker strips. They too become ineffective if there is no longer any contrast between the strip and the roadway.

4.1.7 Loss of visibility on the windscreen

To limit the effects of rain on the windscreen, the wipers evacuate excess water that runs off the windscreen partially obscuring the visual scene. However, between two wipes, the impact of droplets and possibly streaks can be perceived. Water droplets on the windscreen of a vehicle will act as lenses which will disturb the optical path of the light beams before reaching the driver's eyes. One of the main effects is to attract the driver's attention, hide the visual scene and increase glare problems. According to Green (2008), windscreen wipers clean only part of the windscreen, at a given frequency, leaving streaks, and their movement periodically disrupts vision. Regarding the latter claim, Zwahlen (1980) observed that wiper action caused eye movements leading to shorter anticipation distances. In contrast, Cohen & Fischer (1988) showed that wipers do not interfere with the perception of the road scene in relation to the fixation time or saccadic eye movements.

4.1.8 Overall estimation of visibility loss

Research reported by Bhise et al. (1981) examined the sight distance of target vehicles during periods of natural precipitation by day. The participants, aboard a parked or moving vehicle, declared the time when they detected the target while their wipers were on or had recently stopped. They reported that during showers, detection distances significantly decrease as ambient lighting decreases. In addition, they observed at the same time, a decrease in the sight distance with an increase in rainfall rate. Finally, drivers on board moving vehicles have lower sight distances relative to those on board parked vehicles, which is partly related to greater precipitation intensity on the windscreen. Based on their experiments, they proposed a model expressing the sight distance of other vehicles through the windscreen in rain according to rainfall rate and background luminance:

$$D = c_0 (rt)^{-c_1} \, e^{c_2 L_f}$$

where c_0, c_1 and c_2 denote positive constants, the product rt denotes rain build-up on the windscreen, with r rainfall rate and t the duration of the period without wipers, and finally L_f, the background luminance.

According to Andrey et al. (2003), driver visibility decreases (approximately linearly) when the rainfall rate increases. This effect is mainly due to the presence of a film of water on the windscreen rather than a reduction in atmospheric visibility. This reduction is greater for low ambient brightness, low-speed wiper systems, small droplets and splashes from other vehicles (Ivey, Griffin III, Wambold, Zimmer, & Ross Jr, 1984; OECD, 1976).

4.1.9 Characterisation of the "spray" phenomenon

Water jet caused by vehicles are divided into two categories: splash and spray effect (Paschkewitz, 2006). The splash effect is due to large water drops projected by the wheels as splashes. The spray effect is due to the projection of micro-droplets coming from the collision between the vehicle and water suspended in the air, or from the separation of the water jet formed at the rear of tires. Splash and spray consequences on safety are difficult to assess (Paschkewitz, 2006). However they are (Dumas & Lemay, 2004)Although studied in the literature (Dumas & Lemay, 2004; Paschkewitz, 2006; Radovich, 2010), spray and splash phenomena are not finely characterized. Spray effect is the only one which has a strong impact on visibility as shown on Figure 4.4. This literature review is therefore limited to the spray.

Figure 4.4: A mild case of reduced visibility due to the splash and spray of a typical heavy truck. From Dumas & Lemay (2004).

The standard SAE J2245 specifies the conditions for measuring the intensity of the spray phenomenon but it is difficult to put into practice. Moreover, wind, road type, water film thickness, vehicle speed, vehicle type and shape or tire type have an impact on the characteristics of the induced spray (Dumas & Lemay, 2004). Finally, spray effect is not homogenous and it is not the same in any direction (Radovich, 2010). Although some studies have different conclusions (Paschkewitz, 2006), some characteristics of the spray phenomenon have been modelled or measured.

From a macroscopic point of view, the spray phenomenon has a significant impact on visibility. Within the meaning of Beer Lambert law, visibility may be reduced to 90% at a distance of 20m behind a truck by the spray phenomenon (Paschkewitz, 2006). Dumas & Lemay (2004) reported a loss of visibility of up to 80% around a moving truck.

From a microscopic point of view, the droplet size distribution was evaluated, but not their velocity. The droplet size resulting from the spray phenomenon is of the order of $[0.05\ mm - 0.5\ mm]$ according to numerical simulations (Paschkewitz, 2006). Spray measurements made on a laboratory wheel show droplet size distributions between 0 and $4\ mm$ (Figure 4.5). Most present droplet diameters in the spray are between 0 and $0.5\ mm$. These results are consistent with the values obtained by Paschkewitz (2006). Finally, the higher the rolling speed is, the thinner the droplet size is as shown in Figure 4.5. It can be assumed that this higher speed will give a larger water spray.

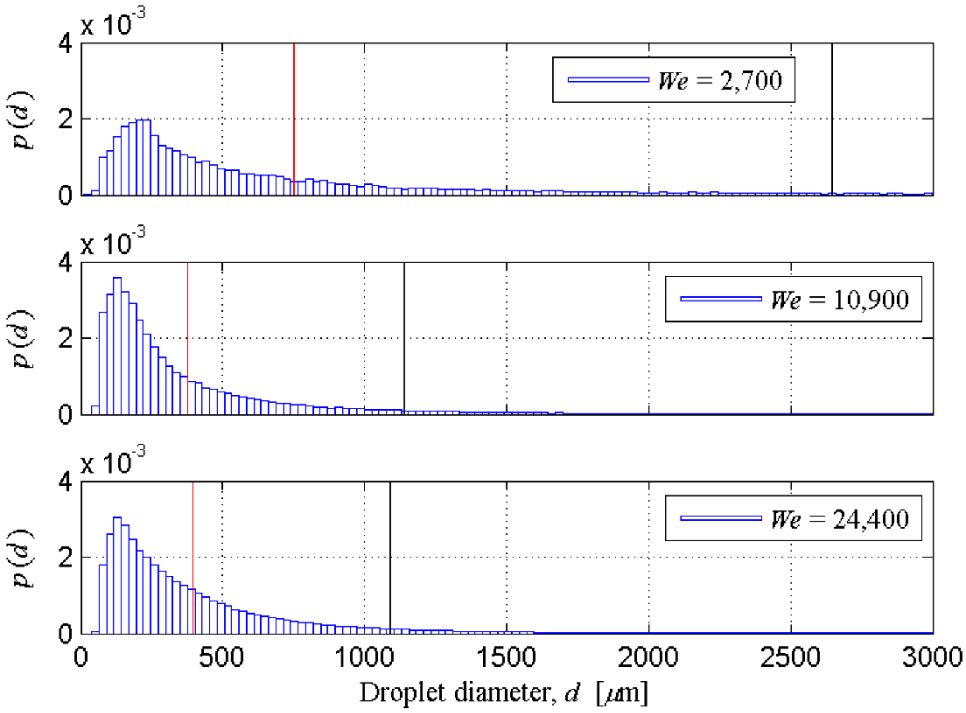

Figure 4.5: Droplet size distributions behind a rolling tire (— global mean droplet diameter, — extent of most probable size range). W_e is the Weber number, it is related to the rotation speed of the wheel. From Radovich (2010).

In conclusion, although many studies exist in the literature, no validated characterization or models of the spray phenomenon exist. Moreover, many parameters have to be taken into account: wind conditions, speed, road type, tire type, vehicle type… However, there are overlapping data concerning the loss of visibility and size of the drops. From a microscopic point of view, the droplet size distribution is between $50\ \mu m$ and $4\ mm$ and it has a peak around $250\ \mu m$. From a macroscopic point of view, the visibility may be reduced by 90%. This is a reason for further investigation.

4.2 Macroscopic parameter of rain: rainfall rate

The macroscopic parameter used to measure the "quantity" of rain is the rainfall rate. Rainfall rate is generally expressed in mm/h.

Rainfall rate is characterized by the height of water that falls during a rainy period. It represents the volume of water falling on a surface per unit time. The unit of rainfall rate is millimetres per hour (mm/h): 1mm/h = 1L/m²/h.

In terms of the kinds of precipitation, the following can be distinguished:

Stratiform precipitation: this type of precipitation covers a large area, lasts for a long time but is of low intensity; it occurs in low pressure areas and valleys and is associated with stratus cloud types;

Convective precipitation: this type of precipitation covers small areas, does not last for long, is intense, very localized and produced by convective instability of the air; it is associated with the cumulus cloud type and may occur in connection with a stormy situation.

The following table from standard NF P 99-320 gives the range of rainfall intensities (in mm/h):

Table 4.1: Standard NF P 99-320 gives the range of rainfall intensities (in mm/h).

	Precipitating fog	Rain	Drizzle	Snow water equivalent	Hail
Very light	---	< 0.1	< 0.1	< 0.1	---
Light	---	0.1 ≤ I < 2.5	0.1 ≤ I < 0.25	0.1 ≤ I < 2.5	---
Moderate	---	2.5 ≤ I < 7.5	0.25 ≤ I < 0.5	2.5 ≤ I < 7.5	---
Strong	---	I ≥ 7.5	I ≥ 0.5	I ≥ 7.5	---
Record in mainland France	---	25	---	---	---
Cyclone (Réunion)	---	250	---	---	---

To better portray rain with respect to their effect on sensory data, droplet size and number of drops may be associated with the rainfall rate. This makes it possible to better distinguish rain categories. For example, drizzle is characterized by smaller droplets than those that make up rain. The size of the droplets determines their fall velocity.

From a mesoscopic point of view, the size or velocity distribution of each droplet must be known. These parameters will have an impact on the images acquired in rainy conditions. Several pieces of research have focused on analysing these parameters and attempting to model the relationship that exists between them.

4.3 Micro-physical parameters of rain

4.3.1 Particle size distribution of raindrops

Particle size analysis is the study of the statistical distribution of sizes of a collection of finite elements of natural or fractionated material, here: raindrops. Depending on its origin, the precipitation observed may have different characteristics, particularly in terms of the structure and distribution of the droplets according to their diameter. Raindrops generally have diameters in the millimetre range, varying from 0.5 to 5 mm, thus about 100-1000 times the size of fog particle size.

As a first approximation, particle size distribution is expressed by a power law of the following form, known as the Marshall & Palmer (1948) relation:

$$N(D) = N_0 . D^{\eta} . e^{-\Lambda . D}$$

where $N(D)$ is the concentration of droplets per diameter interval and per unit volume (in cm-4 or m-3.mm-1), N_0 is the intercept and Λ is the slope of the curve (inverse of the average diameter of the drops). The two parameters N_0 and Λ are dependent on rain type: slightly for the first and more significantly for the second. As a first approximation (according to Marshall and Palmer (1948)), it is assumed that:

N_0 is constant and close to N_0 = 0.08 cm-4

Λ is a constant related to rainfall rate by: $\Lambda = 41 * \mathrm{I}^{-0.21}\mathrm{cm}^{-1}$

I is the precipitation rate in mm/h

η is a constant equal to 1 in the case of uniform rain (conventional)

Studies have made it possible to validate the Marshall-Palmer relation, while showing some discrepancies (Desaulniers-Soucy, Lovejoy, & Schertzer, 2001). Other laws linking rainfall rate to the distribution of droplet size exist (Feingold & Levin, 1986; Ulbrich, 1983). Some, however, use additional parameters which make them difficult to use for digital simulation. In all cases, the droplet size rarely exceeds 6mm although larger droplets may exist (Allamano, Croci, & Laio, 2015). Barnum, Kanade, & Narasimhan (2007) even makes the approximation of a droplet size distribution that is uniform only between 1mm and 3mm in diameter.

In this model the droplets are considered as spheres. Some models refine this assumption by specifying the shape of the droplets analytically (Andsager, Beard, & Laird, 1999; Beard & Chuang, 1987; Chowdhury, Testik, Hornack, & Khan, 2016).

4.3.2 Droplet fall velocity

Various laws are proposed to represent the relationship between the size and the velocity of droplets. Free-falling droplets fall in a stable condition after falling 9m. The forces of gravity and air resistance cancel each other out and the velocity becomes constant: we then speak of terminal fall velocity. Different formulas connect droplet size to their terminal fall velocity. Here the phenomenon of wind is ignored. The terminal fall velocity is therefore vertical in this type of formula. The impact of wind, ignored here, has been analysed in several works (Tokay & Beard, 1995; Van Mook, Wit, & Wisse, 1997).

A raindrop is subjected to three forces:

Weight : $P = mg = \rho_{water} V g$
Archimedes Thrust: $\pi = \rho_{air} V g$
Friction forces due to air drag: $f = \frac{1}{2} C_x \rho_{air} v^2 S$
with:
V, the volume of the droplet comparable to a sphere of radius R, $V = {}^4/_3 \pi R^3$
S, the friction surface comparable to a circle of radius R, $S = \pi R^2$
C_x, the aerodynamic drag coefficient, estimated = 0.5

The terminal velocity of falling droplets, or equilibrium velocity, is achieved when there is balance between the forces (Newton's law). A relationship is obtained of the type:

$$v = k\sqrt{D} \text{ with } D \text{ in mm}$$

Based on the work of Rodgers et al. (1974), the experimental value of k is 3.5. Other authors proposed little different relations (Atlas, Chowdhury et al., 2016; Foote & Toit, 1969; Garg & Nayar, 2004, 2007; Gunn & Kinzer, 1949; Villermaux & Eloi, 2011). The curves obtained for the different formulas are shown in the following figure.

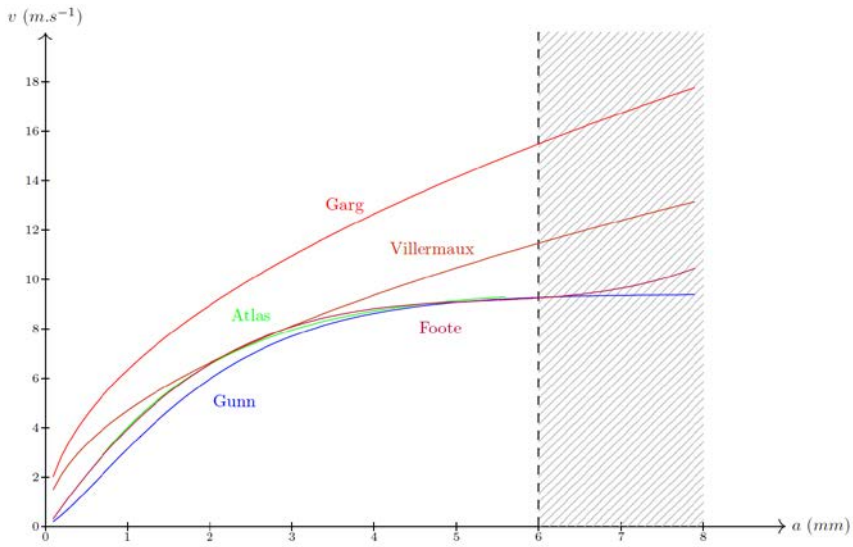

Figure 4.6: Terminal droplet velocities according to proposed formulas.

4.4 Rain sensors

We will present successively:

- Rain gauge type sensors, which measure the macroscopic parameters that make up water level and rainfall rate.
- Disdrometers which measure microphysical parameters, size, concentration and fall velocity of droplets
- Weather sensors which include disdrometer functions and add a visibilimeter function.

A recent study in Australia by Kathiravelu, Lucke, & Nichols (2016), gives a bibliographic review of raindrop measurement techniques. From measurement techniques and manual counting during the years 1900 to 1960, he moves to techniques automated by impact and by optical methods.

His analysis focuses on the measurement accuracy for rain composed of large droplets or small droplets, for size, number and velocity. Manual methods cannot provide information on velocity. Automated methods turn out to be inaccurate during heavy rain for characterizing droplet size and velocity. Consequently, errors in the estimate of rainfall rate from disdrometers are possible. It is recommended to

combine traditional rain gauge type sensors with new technologies of the disdrometer type (Kathiravelu et al., 2016). New camera-based sensors are being developed in research centres (Molinié et al., 2016).

The different types of sensors are presented below.

4.4.1 Rain gauges

Rain gauges are used to measure the amount of water that has fallen during a given time (macroscopic parameter).

It is measured vertically and corresponds to the volume of water fallen on the ground. It is expressed as the quotient of a volume of water precipitating through a section. This volume of water is expressed as a water level over a surface of one m2: 1 mm of precipitation in fact corresponds to 1 litre of water per square meter.

Precipitation level can be measured using a rain gauge. Rain gauges used by weather departments are recording rain gauges with two small buckets whose capacity is equivalent to 0.1, 0.2 or 0.5 mm of water. The amount of precipitation is measured by the number of times the buckets tip, detected by a mechanical or optical system. Based on the duration of measurement, the water level is then converted into rainfall rate in mm/h.

Figure 4.7: Recording rain gauge of the Précis Mécanique type. © Météo-France.

4.4.2 Impact disdrometers

A disdrometer is an instrument used to measure the diameter distribution of hydrometeors and their fall velocity (microscopic parameter).

An impact disdrometer is a force sensor that transforms the impact caused by the kinetic energy of the hydrometeor hitting it into an electric pulse whose amplitude is proportional to its mass and its fall velocity.

From this distribution, rainfall rate can then be estimated by calculating. The signal resulting from the impact of the droplet is proportional to its volume, and, after integrating all the droplets, the total cumulative rainfall and the duration of each precipitating event (the count taking place from the impact of the first droplet) can therefore be deduced.

By way of illustration, the diagram in Figure 4.8 shows how the Raincap probe works.

Figure 4.8: Vaisala Rain Cap disdrometer (Vaisala, 2015).

4.4.3 Optical disdrometers

An optical disdrometer uses a light beam which is broken when a hydrometeor passes through it. Any wavelength can be used (visible, infrared, etc.). In order to minimize light scattering by air and precipitation, lasers are now most often used. When a droplet passes through the light beam, the light energy received per the sensor's photodiode decreases. The amplitude and duration of the signal caused by the passing droplet are proportional to the vertical section and the residence time (fall velocity) respectively of the droplet in the light volume.

Each particle analysed is then placed in a class of diameters and velocities (of width defined by the manufacturer). The fall velocity of the droplet across the beam is derived from the ratio between the height of the beam and the signal duration (i.e. the residence time).

Figure 4.9 illustrates the discrimination of hydrometeors from the measurement of their size and fall velocity.

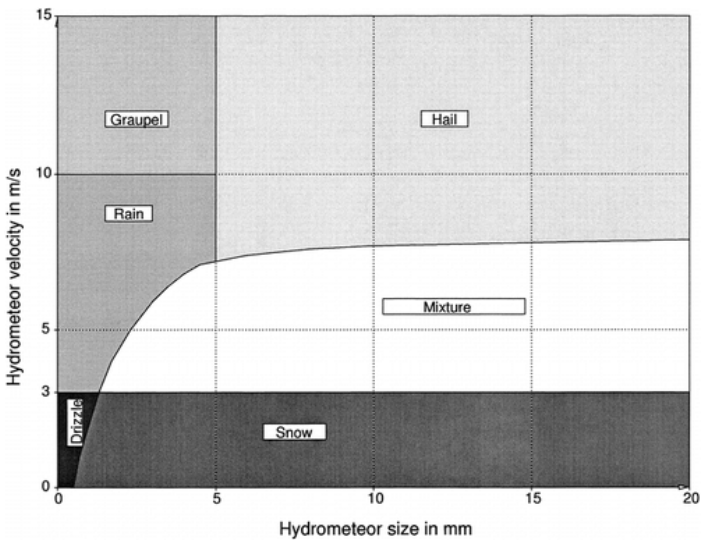

Figure 4.9: Hydrometeor recognition by means of raw data for the Parsivel disdrometer. From Löffler-Mang & Joss (2000).

The World Meteorological Organization (WMO) has defined a classification of precipitation and an encoding system that is used by most disdrometers.

1. Drizzle

Intensity	Rain rate [mm/h]	SYNOP ww
light	≤0.2	51
moderate	0.2…0.5	53
strong	≥0.5	55

2. Drizzle with rain

Intensity	Rain rate [mm/h]	SYNOP ww
light	≤0.2	58
moderate	0.2…0.5	59
strong	≥0.5	59

3. Rain

Intensity	Rain rate [mm/h]	SYNOP ww
light	≤0.2	61
moderate	0.5…4.0	63
strong	≥4.0	65

4. Rain, drizzle with snow

Intensity	Rain rate [mm/h]	SYNOP ww
light	≤0.5	68
moderate	>0.5	69

5. Snow

Intensity	Rain rate [mm/h]	SYNOP ww
light	≤0.5	71
moderate	0.5…4.0	73
strong	≥4.0	75

6. Snow grains

Intensity	Rain rate [mm/h]	SYNOP ww
light	≤0.5	77
moderate	0.5…4.0	77
strong	≥4.0	77

7. Freezing rain

Intensity	Rain rate [mm/h]	SYNOP ww
light	≤0.4	87
moderate	>0.4	88

8. Hail

Intensity	Rain rate [mm/h]	SYNOP ww
light	≤7.5	89
moderate	≥7.5	90

Figure 4.10: SYNOP (surface synoptic observations) classification of the type and intensity of precipitation according to FM-12 by WMO (Degreane Horizon, 2016).

Most disdrometers can:

- Identify 8 types of precipitation according to the previous table: drizzle, drizzle mixed with rain, rain, sleet, snow, snow grains, icy rain, hail
- Measure the particle size (diameter) of precipitation
- Measure the fall velocity of particles
- Measure the rate of precipitation (mm/h), or classify the types of precipitation rate (light, moderate, strong) according to the previous table.

Three systems are outlined below.

- The OTT disdrometer - Parsivel

Figure 4.11: The OTT Parsivel disdrometer.

- The Thies Clima disdrometer

Figure 4.12: The Thies Clima disdrometer (Thies Clima, 2016).

- The CIMEL Electronique disdrometer

Figure 4.13: The CIMEL Electronique disdrometer (Cimel, 2016).

This disdrometer is the one that was developed with Précis Mécanique. It uses an infra-red LED which passes through a double slot to generate a double beam. After passing through the measurement zone, the double beam is focused onto two photodiodes by a double Fresnel prism. A raindrop falling through the beams causes a successive intensity variation of each photodiode.

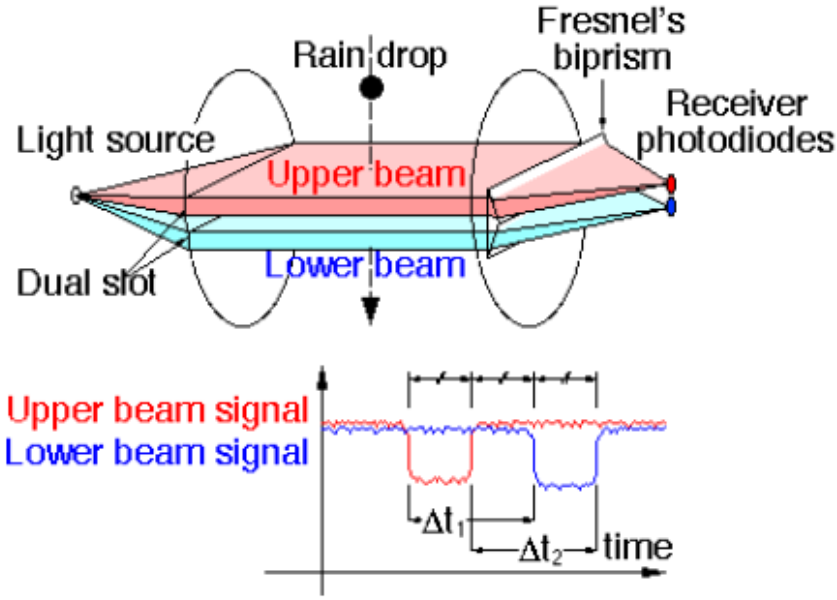

Figure 4.14: How the CIMEL Electronique disdrometer works. From Armetta (2006).

It cannot classify the different types of precipitation, but it measures the particle size of precipitation: Size (diameter) of the particles ranging from 0.1 to 20 mm

4.4.4 Other sensors - present weather sensors

In recent years a new generation of sensors, called "present weather sensors" has appeared. Like the most sophisticated disdrometers, they indicate the main characteristics of hydrometeors. They detect the presence of precipitating hydrometeors and attempt to qualify them: drizzle, rain, freezing rain, snow, sleet and hail, with an indication of their intensity. Some additionally give indications as to visibility (meteorological optical range). All weather departments are currently taking an interest in these sensors because they can make it possible not to use a human observer for observing the weather, called *present weather*.

The present weather sensor is actually a set of sensors associated with software that merges data; by cross-referencing information, it can discriminate between different types of precipitation. Compared to disdrometers, which classify precipitation by particle size and fall velocity, they also measure loss of atmospheric visibility, i.e. they quantify fog density. They therefore measure:

- visibility (MOR: Meteorological Optical Range)
- the size, quantity and velocity of precipitation
- relative humidity
- air temperature
- and possibly wind speed

Analysis of these parameters can output:

- 8 types of precipitation: drizzle, rain, snow grains, snowflakes, hail, ice pellets (hailstones), sleet, freezing rain and freezing phenomena
- 4 types of obscuration: fog, steam, haze (smoke, dust particles in suspension, sand), and absence of obscuration (atmospheric clarity)
- the particle size of precipitation:
- the fall velocity:
- the rate of precipitation:
- meteorological visibility

Some examples are given below:

- The PWS100 by Campbell

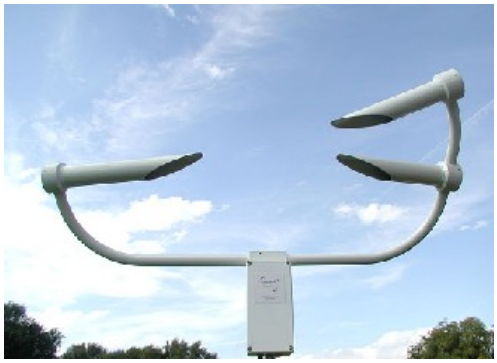

Figure 4.15: The PWS100 sensor by Campbell (2016).

The PWS100 (figure above) uses a new optical system based on a light source that forms a structured volume for detection. This is used to accurately measure the velocity and size of falling precipitation. This system improves the performance of present weather sensors and optical disdrometers using techniques derived from "Laser Doppler Anemometry" (LDA) to more accurately determine the velocity and size of particles to ± 5%. The PWS100 allows classification of particles such as rain, snow, hail and ice, giving the velocity and size of the particles and also by using the signal structure, which differs significantly between a liquid and a solid, depending on the type of precipitation.

- The VPF730 by Biral

Figure 4.16: VPF730 by Biral (2016).

It has a very fast sample rate of the order of laser pulses.

- The PWD12 (and PWD22) by Vaisala

Figure 4.17: The PWD12 sensor by Vaisala (2016).

The PWD 12 and PWD 22 Present Weather Sensors by Vaisala identify the type of precipitation, accurately indicating its water content using a capacitive device (an element of the Raincap® sensor by Vaisala) and combining this information with a forward scatter technique and temperature measurements. These three independent measurements are processed in sophisticated algorithms to produce an accurate assessment of the type of weather according to the WMO and NWS code tables.

Precipitation measurement is based on Vaisala Raincap® technology that detects the impact of each raindrop. The signals from the impacts are proportional to the volume of the droplets. As a result, the signal from each droplet can be directly converted into cumulative rainfall. It is therefore a present weather sensor that provides precipitation rate but not particle size.

5 Natural ice and snow

5.1 Characteristics of snow precipitation

The present weather parameter "snow" is defined as "precipitation of snow crystals, mostly branched in the form of six-pointed stars". The intensity of snow fall can be characterized by reporting the respective reduction in visibility. In the U.S. Federal Meteorological handbook, snow fall intensity has been divided into three categories:

Table 5.1: Three snow categories according to the U.S. Federal Meteorological handbook.

Snowfall Intensity	Visibility criteria
Light	Visibility > 1.6 km
Moderate	0.8 km ≤ Visibility ≤ 1.6 km
Heavy	Visibility < 0.8 km

Another possibility in describing snow fall intensity is to utilize the equivalent water content. A general rule-of-thumb is that a snowfall incident has 10% of the water content of a rainfall incident, if these two incidents cause a similar reduction in overall visibility. The Word Meteorological Organization (WMO) publication WMO-No8, "Guide to Meteorological Instruments and Methods of Observation", relates snow intensity and water equivalent content as follows:

Table 5.2: Three snow categories according to WMO.

Snowfall Intensity	Criteria for water equivalent (WE) content
Light	WE < 1.0 mm h-1
Moderate	1.0 mm h-1 ≤ WE < 5.0 mm h-1
Heavy	WE ≥ 5.0 mm h-1

The microphysical properties of snow (such as distributions for snowflake size and mass) vary and have been studied in literature. However, it is often more practical to describe snowfall by using either the reduction in visibility or equivalent water content.

5.2 Instrumentation for measuring snow precipitation

The various properties of snow precipitation are typically characterized by using optical weather instruments. This operation principle of these instruments is based on measuring the reduction in signal transmittance due to precipitation (disdrometers), or alternatively they are based on measuring the increase in signal scattering due to precipitation (forward-scatter based present weather detectors). It is possible to indicate quantities such as reduction in visibility, estimated equivalent water content of snow precipitation, and particle size.

Besides optical instruments, a direct measurement of equivalent water content of snow precipitation can be realized with the traditional heated rain gauge.

Figure 5.1: An example of a present weather detector based on measuring the forward-scattered light.

5.3 Categorizing different road surface states

Road surface state reporting generally refers to measuring and categorizing the prevailing road surface state to classes such as dry, wet, icy etc. In general, the aspects that affect and dictate the state of a road surface may be divided to three different categories:

- **Environmental aspects** such as air temperature, air dew point, solar radiation, type of precipitation, road surface temperature etc. naturally have an impact on road surface status.
- **Road winter-maintenance efforts** are typically carried out in order to improve road surface conditions and driving safety. Examples of maintenance activities are ploughing of snow, and the spreading of de-icing compounds in order to lower the effective freezing point of the water on the road.
- **Traffic-related aspects** such as traffic intensity may affect the surface status as well. For example, car tires compact snow, and occasionally "polish" snowy roads in wintertime so that friction is slowly reduced. Another example is that intense traffic tends to displace the winter-time de-icing compounds on the road surface, hence reducing the effectiveness of de-icing.

In what comes to road surface states, the European Standard EN 15518-3:2011 suggests the following classification and definitions:

Table 5.3: Surface states classification according to EN15518-3:2011.

Surface state	Description
Dry	No humidity over the sensor
Moist	From 0.01 mm water thickness over the sensor
Wet	From 0.2 mm water thickness over the sensor
Streaming water	From 2 mm water thickness over the sensor
Slippery	Detection at least of the presence of partly or wholly solidified aqueous solution over the sensor

Practices in categorizing road surface states vary somewhat between instrument manufacturers. Some optical remote road state instruments have the capability to detect and report more surface state categories than mentioned in the EN 15518 standard.

For practical road winter-maintenance purposes, experience has shown that the following surface state categorization is useful:

Table 5.4: Winter-maintenance practical surface states.

Surface state	Description and visual observation
Dry	The surface is dry.
Moist	0.015 mm < Water thickness < 0.045 mm. Visual observation on surfaces like asphalt and concrete is that surface has become darker due to moisture, but it is not yet clearly wet.
Wet	Water thickness > 0.045 mm. Visual observation at the threshold is that in addition to the surface being clearly darker due to moisture, it starts to appear visually wet (often possible to state by noticing the characteristic visual reflection properties of a wet surface).
Ice	Ice thickness > 0.015 mm. A threshold which is often undeterminable visually by an observer, but is already at the verge where ice starts to have a reducing effect on friction.
Slush	A simultaneous combination of liquid water and snow. Visual observation is typically related to wet snow.
Snow	Snow thickness > 0.03 mm water equivalent. Visual observation at the threshold is typically that there appears to be a slight amount of snow on the surface and hence it is not dry, but the observer still sees more surface than snow.
Frost	A detectable amount of ice-like element on the road. Surface temperature has been below air dew point temperature, and as a consequence, frost has formed from the direct deposition of airborne humidity to solid form. Typical visual observation is a light "haze". There are occasions where even a slight amount of frost reduces friction notably.

5.4 The impact of road surface state on friction

The level of prevailing friction between the vehicle tire and a road surface of a given surface state is, in practice, a somewhat complex topic, and generally affected by the following aspects:

- **Road surface state**, for example, thickness of prevailing layers such as ice has a big impact on friction.
- **Properties of the vehicle tire**, for example, tire type (such as Nordic studded winter tire, summer tire, etc.) and tire conditions (new, old etc.)
- **Speed of the vehicle**, for example, higher speed increases the risk for aquaplaning with thick water layers.

- **Macro-physical properties of the road surface**, for example, surface roughness of asphalt.
- **Automated vehicle functions,** for example, the ABS not being able to react and adapt fast enough to road surface changes thus causing accident risk or having large safety margin by reducing speed to inconvenient level.

The main relationships between road surface states and prevailing friction levels can briefly described as follows:

- **Dry road** has the maximum available level of friction for that particular surface type. The absolute friction value has a smallish dependency on macro-physical properties of the surface and the tire, but in general, the level of friction on dry roads is overall very good and not problematic for the driver. As the surface becomes more and more slippery (due to ice, snow etc.), the role of road surface macro-physical properties in determining friction reduces further, and aspects such as surface state, tire type and vehicle speed then dominate in determining friction levels.
- **Wet, icy, snowy, frosty and slush surfaces:** It can be summarized that increasing film thickness for all these elements reduce friction, but in way that is characteristic to each element. Some key aspects of practical importance are given below:
  - **Wet road surfaces** may be problematic due to the increased risk of aquaplaning. In addition to the amount of water itself, this risk is also dependent on vehicle speed. Another issue specific to wet surfaces is that tires start to lift and spray water mist around when the water film thickness is the order of 0.2 mm or greater. With dense traffic, this fine droplet spray may notably reduce visibility at the eye-level of drivers, even if the atmospheric visibility beside the road is good.
  - **Icy road surfaces** are one of the main reasons for extremely low friction levels. Ice starts to reduce friction with film thickness around 0.03 mm. With ice thickness in the order of 0.2 mm, the friction is already reduced to minimum and the surface is extremely slippery. This is why it is important that road state instruments have a good sensitivity to reliably detect thin layers of ice. Also cases with water on top of ice need to be addressed.
  - Also for **Snowy surfaces,** friction reduces for increasing thickness of snow. However, for thick and compacted snow layers, the typical minimum friction level is still notably higher than that of ice, making snowy roads more manageable and more predictable for the driver.
  - **Frosty surface** is characteristic in that even thin layers of frost can make the road extremely slippery.
  - **Slush surface** has properties somewhat similar to wet surface. The tire tread pattern can displace small amounts of slush (and hence the friction is relatively good), but large amounts of slush reduce friction further and may lead to an event similar to aquaplaning.

5.5 Instrumentation for measuring surface states

From the viewpoint of instrumentation, road surface state measurements can be divided to two main categories:

1. Stationary installations of road weather station networks. Classification of prevailing road surface state is typically one output that these stations report. Atmospheric measurement results (such as air temperature, precipitation data etc.) may be combined with the results of dedicated surface state sensors in order to classify the road state. The state sensors can be further divided to two main categories:

    a. Intrusive sensors, which are mounted in the road at the level of pavement surface, and hence provide an in-situ measurement for parameters such as film thickness and conductivity.

    b. Non-intrusive i.e. remote sensors, which in practice are optical sensors, capable of characterizing for example film thickness and surface states by spectroscopic means. These are typically mounted beside the road on the road weather station mast, and monitor the road at a 5-20 m measurement distance.

2. Mobile installations. In this group, a remote sensor is mounted on a vehicle, and it measures the surface state as the vehicle drives on. The operation principle as such is similar to the spectroscopic approach of stationary units. Installation practices vary, and the monitoring distance is in the order of 20 cm – 2 m. Some mobile units also incorporate measurements of additional parameters, for example air humidity, air temperature and surface temperature.

The remote road state sensors are also capable of estimating the prevailing level of friction. However, the operation principle of optical road state sensors is such that they primarily detect the state of the surface, and hence friction is a derived parameter. Commercial examples of more direct ways of measuring the friction would include, for example

- incorporating an additional and dedicated measurement wheel which is in contact with the surface, or
- measuring the deceleration during full power braking, and respectively determining the friction from the magnitude of available maximum deceleration.

Figure 5.2: Example of optical remote (non-intrusive) sensors: remote surface temperature sensor on the left, remote surface state sensor on the right.

Figure 5.3: Example installation of intrusive surface state sensors.

6 Available methods to simulate fog and rain

6.1 Simulation of fog

To generate artificial fog, two methods are employed. The first is based on the principle of natural generation, and uses thermodynamics to saturate air with water vapour and produce fog by changing the temperature and humidity of the volume. The second is based on a mechanical principle: within a nozzle, the pressurized water is split into micro droplet that is projected in the volume of production. A state of the art on both production methods is proposed in the following sections. It updates a previous state of the art (FOG Report, 2003).

6.1.1 Thermodynamic systems

Several thermodynamic systems for fog production could be identified (Khlystou, Kos, & ten Brink, 1996; e.g. Singh, 2011), see Singh (2011) for a fuller list. However, as these systems require precise temperature control, low temperature values, the energy cost is too important to be viable for large-sized rooms. For example, the Fog System Research Laboratory (FRL), developed by Indian Institute of Technology Kanpur in India, has a volume of only 0.8m3 (Singh, 2011). The other identified installation, High Flow Turbulent cloud chamber developed at the Energy Research Foundation (ECN) in Netherlands has a volume of 1.25m3 (Khlystou et al., 1996). Thus, these dimensions do not allow considering the use of this type of fog simulator for road applications where the required volume is of the order of a few hundreds of cubic meters.

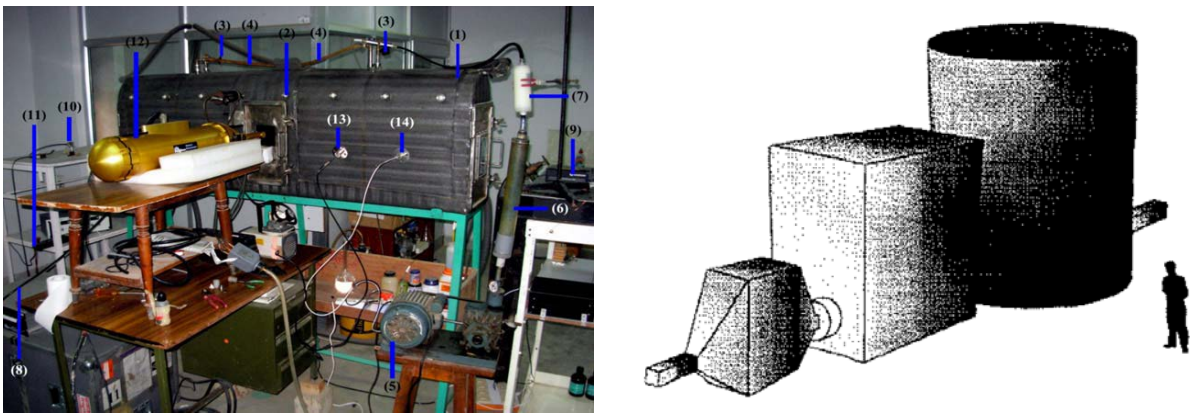

Figure 6.1: Two thermodynamic systems for fog production. Left : Fog System Research Laboratory (FRL) (Singh, 2011). Right : High Flow Turbulent cloud chamber (Khlystou et al., 1996).

In addition to these systems, there are many other climate room systems, but without the ability to create fog or mist. Although climate room allow the control of humidity and temperature, water saturation remains too low for the production of fog. As simulated conditions are less critical, climatic rooms are larger than thermodynamic systems for fog production, but they are out of the scope.

6.1.2 Mechanical systems (by hydraulic injection)

The other way to simulate fog is based on a mechanical principle. Due to nozzles, pressurized water is sprayed in micro-droplet in the enclosure. This solution, considerably cheaper than the first one, allows the design of much larger installations. Most of the identified installations are then used for studies in aeronautics or automotive sectors. Specific installations dedicated to automotive transport are listed below.

6.1.2.1 Virginia Smart Road

The Virginia Smart Road (VSM) is a 3.5km long two-lane road. It is operated by the Virginia Tech Transportation Institute. This road is made available for research for various transport applications (lighting, communication, pavement…). It has fog and rain production systems. For production, 75 towers with nozzles are spread over 800m along the way. They allow producing fog if conditions are favourable (no wind and low temperature). The visibility range offered is 3 to 90m. Only one scientific publication of a study using the fog feature of this platform could be found (Blanco & Hankey, 2005). This study focuses on visibility at night and in fog condition. It is complemented by other studies with other weather conditions.

Figure 6.2: Photos of the VSM during fog production. From Blanco & Hankey (2005) and Virginia Tech Transportation Institute (2016).

6.1.2.2 The PWRI weather Environmental test Track

The PRWI owns a test track in Tsukuba (Japan) since 1998. This track has been used for challenge Demo2000 (Huang, Tan, & Bu, 2010). This 6km long track contains a section with a tunnel for generating artificial fog and rain (Colomb et al., 2008). This facility dedicated to the adverse weather conditions measure 200m long, 9.8m wide and 6.9m high (Public Work Research Institute, 1998). The tunnel is made of a transparent structure. It is equipped with nozzles for spraying fog. This facility allows reproducing fog visibility from 10 to 100m.

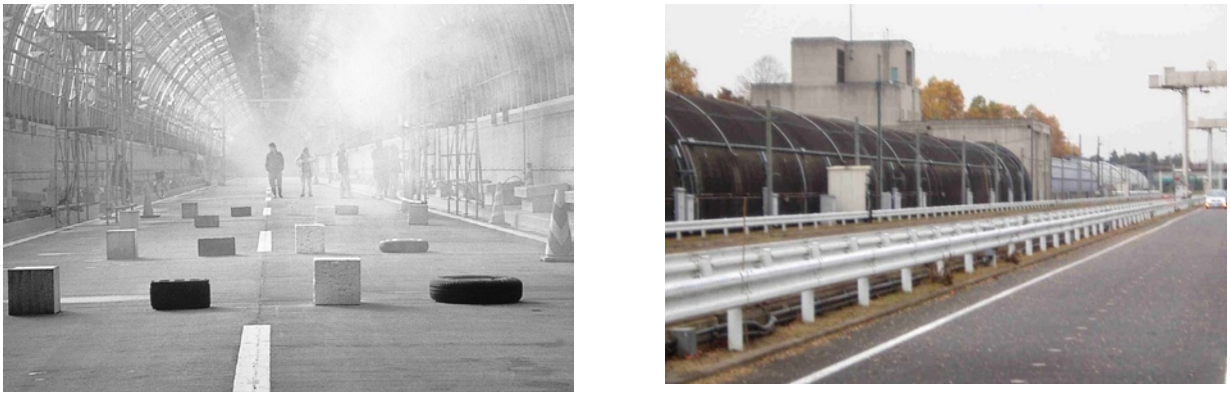

Figure 6.3: View of the interior of the tunnel during the fog production (left) (Yamawaki, Yamano, Katogi, Tamura, & Ohira, 2000) and of the exterior of the production tunnel (right) (Nielsen, Bendtsen, Andesen, & Larsen, 1999).

6.1.2.3 Cerema Fog & Rain R&D Platform

The Cerema has an infrastructure for the generation of fog and rain in Clermont-Ferrand (France). This 31m long platform includes a 15m long fixed part (tunnel) and a 16m long lightweight part (greenhouse) with a transparent (daytime) or opaque (night time) cover. The platform has a width of 5.5m and a height of 2.4m. An observation post is located at the end of the platform, in order to install the equipment outside of the wet area during testing. Fog is produced by nozzles and monitored following a real time measurement of the visibility by transmissiometers. Thus, the visibility can be kept constant in time for fog between 5m and 200m. The droplet size distribution is controlled in this platform. Different distributions similar to those obtained for some natural fog are thus available and measured thanks to an optical granulometer (Colomb et al., 2008). The spatial homogeneity of fog has also been validated on this infrastructure (Colomb et al., 2008).

Figure 6.4: Night view with fog production (left) (Colomb et al., 2008) and global view of Fog & Rain R&D Platform (right).

6.1.3 Conclusions

Several essential parameters for the fog simulation for automotive applications have been identified through this bibliography: the size of the production area (minimum tens of meters in length), the visibility range offered by the infrastructure (minimum 0m-200m), the droplet size distribution of produced fog, spatial and temporal uniformity of the fog.

Two methods exist to produce fog: thermodynamic and mechanic. From an energy point of view, the thermodynamic-based solution is not possible for the volumes required for automotive applications. All existing infrastructure for these applications are therefore based on the mechanical principle. Only three such facilities have been identified: VSR (USA), PWRI (Japan) and Cerema (France).

Visibility range varies an infrastructure to another. However, it always reaches a range of a few meters to a few hundred meters.

The droplet size distribution is a key criterion for performing detailed analyses, especially since some droplets can produce interacting with light. Only the infrastructure proposed by the Cerema considers this criterion.

Similarly, the Cerema platform is the only which offers results regarding the spatial homogeneity of produced fog. The production of fog on the VSR is available under favourable wind conditions, which leaves to imagine that homogeneity of fog on open sky platform should not be very good.

While the fog produced by the thermodynamic method is stable as long as temperature and humidity are maintained, the mechanical method is not. The droplets gradually evaporate into the air. Addition of new droplet is therefore necessary continuously to maintain a certain visibility. All facilities seem to offer this regulation in order to keep a good temporal stability of fog.

Table 6.1: Summary table of the three fog simulators allowing automotive systems assessment.

	WxLxH (m)	Type	Visibility range (m)	Droplet size distribution	Fog spatial uniformity	Fog temporal stability
VSM	~10x800x~10	Outdoor	3-90			
PWRI	9.8x200x6.9	Indoor	10-100			
Cerema	5.5x31x2.4	Indoor	5-200	x	x	x

The state of the art also helped identify the technical elements for controlling various useful parameters previously mentioned: the type of nozzles, nozzles distribution, quality of the injected water, closed production area, temperature and humidity.

6.2 Simulation of rain

Artificial rain production exists in various fields. The principal use of rain simulation is the study of the behaviour of soil and plants in agronomy. Rain simulation systems in this area are however very small. There are also larger systems whose scope is mainly the automotive transport.

6.2.1 Rain simulators in agronomy

Agronomy is the area in which there is the most rain simulation systems (Claassens & van der Watt, 1993; Dunne, Dietrich, & Brunengo, 1980; Esteves, Planchon, Lapetite, Silvera, & Cadet, 2000; Iserloh et al., 2013; Lassu, Seeger, Peters, & Keesstra, 2015; Morin, Cluff, & Powers, 1970). All systems encountered work the same manner. One or more nozzles are positioned on a metal structure a few meters in height. Simulated rain area is approximately of one square meter to a few tens of square meters. The height may be variable, which allows influencing the falling droplet velocity. The height of the identified simulators varies from 1m to 7m. The choice of the nozzles and the water injection pressure is always analysed, taking into account the rainfall rate produced, the droplet size distribution and velocity. Furthermore, although the increase in pressure is often the method used to increase the droplet velocity, the latter has the effect of reducing the size of the droplets and significantly increase the rainfall rate (Morin et al., 1970). Some methods involving cutting intermittently the water injection are then proposed (Morin et al., 1970). More recent methods using meshes under nozzles are proposed to modify droplets characteristics (Carvalho, de Lima, & de Lima, 2014). In agronomy, analysis of droplet velocity and size aims to obtain a ratio of kinetic energy compared to rainfall rate similar of the natural rain ratio. This quantity is indeed important for soil erosion study, although it is out of scope for the automotive application. In agronomy, the goal of these systems is also often to be portable and inexpensive, in addition to reproduce the fairest possible rain.

Although the research work for the development of such systems is particularly rewarding for rain simulation, none of these systems can be used as it is for automotive applications. Indeed, smaller ones only work on one square meter (Claassens & van der Watt, 1993; Dunne et al., 1980; Iserloh et al., 2013; Morin et al., 1970) and bigger ones over a few tens of square meters (Esteves et al., 2000; Lassu et al., 2015). Some systems, however, would be easily adaptable (Esteves et al., 2000).

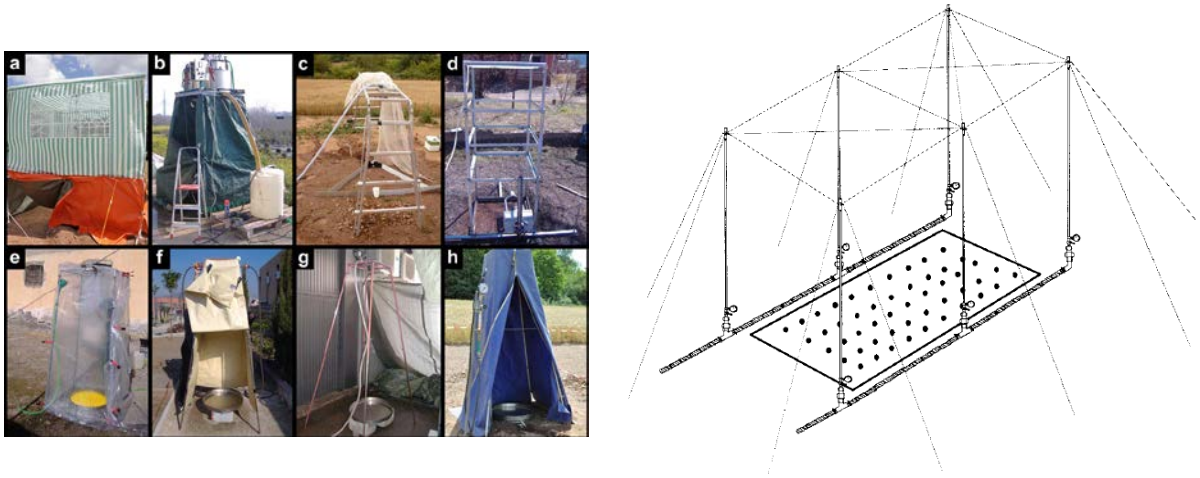

Figure 6.5: Left, some small portable rain simulators reviewed by Iserloh et al. (2013). Right, modular rainfall simulator which could be adapted to automotive applications from Esteves et al. (2000).

6.2.2 Rain simulators for automotive applications

Several rain simulators compatible with automotive studies (large production zone) were identified. The facilities are sometimes complementary to artificial fog simulators.

6.2.2.1 Virginia Smart Road (VSR)

The VSR has already been presented in the previous part because it is also a fog simulator. Rain and fog are produced on the same track of 800m. Proposed rainfall rate ranges from 2 to 63mm/h. The rain is produced by nozzles positioned on the same towers as fog. No data could be found in the spatial uniformity of the rainfall rate, droplet size distribution or drop velocity.

Figure 6.6: Virginia Smart Road rain towers. From Blanco & Hankey (2005).

6.2.2.2 The PWRI weather Environmental Test Track

PWRI platform also allows, in addition to fog simulation, to generate artificial rain. No precise data on the characteristics of the produced rain could be found. A study on the impact of rain on a radar however uses PWRI infrastructure with rainfall rate between 20 and 100mm/h (Yamawaki et al., 2000).

6.2.2.3 The Cerema Fog & Rain R&D Platform

The Cerema Fog & Rain R&D Platform, as VSR and WRI facilities, also simulates rain in addition to fog. The rainfall rate can vary between 10 and 150mm/h. The control of rainfall rate need to be improved, and the rainfall rate need to be widen for the low values. The rain is produced by two types of nozzles which allow varying the droplet size distribution. The water injection pressure is also variable which changes the rainfall rate. Droplet size distribution and droplet velocity are measured using a specific sensor. The spatial homogeneity of the rainfall rate should be improved as well as the duration of the rain.

Figure 6.7: Images of a road scene acquired on Cerema Fog & Rain R&D Platform, with and without rain, daytime and night time (Dahmane et al., 2016).

Figure 6.8: Photograph of a nozzle of the Cerema Fog & Rain R&D Platform during production.

6.2.2.4 *Leibniz Universität Hannover (LUH)*

The LUH has developed an infrastructure to generate artificial rain on a surface of 4m by 3m (Rabiei, Haberlandt, Sester, & Fitzner, 2013). Rain is produced by three types of nozzles located 3m high. Different combinations of nozzles and water injection pressure allow different rainfall rate ranging from 9.2 to 98.1mm/hr. The spatial uniformity of rainfall rate is analysed. However, the droplet size distribution and droplet velocities are not measured. Although this facility is used for an automotive application, its small size makes it difficult to use for various automotive tests.

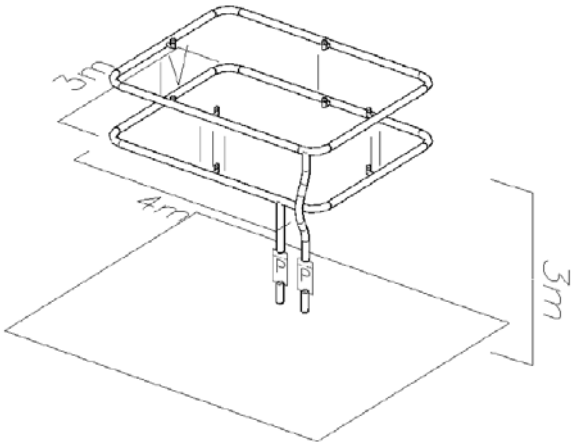

Figure 6.9: Installation sketch of LUH (Rabiei et al., 2013)

6.2.3 Conclusion

The state of the art has identified the parameters that needed to be controlled for a rain simulator: size of the production area (surface and height), rainfall rate range (1 - 100mm/h), droplet size distribution, droplet velocity, and spatial uniformity of rainfall rate (coefficient of uniformity).

The systems used in agronomy provide an accurate control of the rain parameters. Thus, some of them are very good at reproducing natural rain. However, these systems are small and thus inconsistent with a road application.

Four infrastructures specifically dedicated to tests for road applications have been identified. The three facilities identified for the fog simulation are among them.

The infrastructure proposed by the VSR is in open air. Although it possible to obtain much larger production areas outside, natural elements such as wind are then not controlled. However, wind can have a major impact on droplet velocities. Other three identified infrastructures are closed inside a laboratory and thus facilitate the control of all parameters.

Regarding the size of the production area, the installation of LUH is too small with only 4m by 3m.

All rain simulators offer correct rainfall rate ranges. However, the droplet size distribution is measured only on the Cerema platform and spatial uniformity of rainfall rate is measured only on Cerema and LUH platforms.

Table 6.2: Summary table of the four rain simulators allowing automotive systems assessment.

	WxLxH (m)	Type	Rainfall rate range (mm/h)	Droplet size distribution measure	Droplet velocity measure	Rainfall rate spatial uniformity	Spray testing
VSM	~10x800x~10	Outdoor	2-63				
PWRI	9.8x200x6.9	Indoor	20-100				
Cerema	5.5x31x2.4	Indoor	10-150	x	x	~	
LUH	4x4x3	Indoor	9.2-98.1			x	

The bibliography also helped to identify the parameters influencing of the simulated rain: nozzles type, water injection pressure, nozzles distribution, nozzles height, addition of a mesh under nozzles, intermittent cutting of the injection, nozzles orientation. These elements and their influence on the setting of the rain are summarized in the following table.

Table 6.3: Technical elements which are configurable technical versus characteristics of the rain simulated.

	Rainfall rate	Droplet size distribution	Droplet velocity	Rainfall rate spatial uniformity
Nozzles type	x	x	x	x
Water injection pressure	x	x	x	x
Nozzles distribution				x
Nozzles height			x	x
Mesh under nozzles		x	x	x
Intermittent cutting of the injection	x			x
Nozzles orientation			x	x

7 Conclusion

The main effect of fog is to reduce the light transmission through the atmosphere and then reduce the visibility of all the objects to be detected in the road scene. The macroscopic parameter to describe fog is the meteorological visibility distance.

The range of useful meteorological visibility in driving conditions is from 0 m to 400 m. When the meteorological visibility is low, the denser is the fog.

Considering microphysical parameters, the range of the droplet size is from 0.5 µm to 40 µm. Continental fog are having smaller droplets than the maritime fog. Two drop size distributions (small and bigger droplets) are available on the fog and rain platform. These two distributions are similar to natural distribution. Taking account of the droplet size is especially important for infrared based sensors (Lidar, Camera SWIR).

The rain is having various effects on the road environment:

- Reduction of light transmission through the atmosphere (some rain effect is predicted only for the heaviest rain; it is more important than the effect of fog when considering millimetre and sub-millimetre wavelength)
- Road surface reflection and slippery road (depending on surface roughness)
- Reduction of visibility of road markings and signing
- Reduction of windscreen transparency,
- And finally spray production at the interface of tires and road surface. From a macroscopic point of view, the spray phenomenon has a significant impact on visibility and need to be considered in the project.

The total existing rain range extends from 0mm/h (no rain) to 300mm/h (tropical rain). In continental Europe, this range is rather from 0 to25 mm/h (rain storm).

Snow has been defined mostly from the impact of road surface state on friction.

Considering the available methods to simulate fog and rain, only one equipment has been identified on each continent. The Cerema platform in France allows reproducing fog and rain. The DENSE project should allow Cerema to upgrade the rain production system and examine the possibility of spray testing.

8 References

Allamano, P., Croci, A., & Laio, F. (2015). Toward the camera rain gauge. *Water Resources Research*, *51*(3), 1744–1757. https://doi.org/10.1002/2014WR016298

Al Naboulsi, M. (2005). *Contribution à l'étude des liaisons optiques atmosphériques: propagation, disponibilité et fiabilité.* Université de Bourgogne.

Andrey, J., Mills, B., Leahy, M., & Suggett, J. (2003). Weather as a chronic hazard for road transportation in Canadian cities. *Natural Hazards*, *28*(2-3), 319–343.

Andsager, K., Beard, K. V., & Laird, N. F. (1999). Laboratory Measurements of Axis Ratios for Large Raindrops, (1993), 2673–2683.

Armetta, A. (2006). *Etude bibliographique des appareils de mesures de précipitations installés au Col de Porte - juillet à septembre 2006*. Laboratoire d'Etudes des Transferts en Hydrologie et Environnement (LTHE).

Avotniece, Z., Klavins, M., & Lizuma, L. (2015). Fog climatology in Latvia. *Theoretical and Applied Climatology*, *122*(1-2), 97–109.

Babari, R. (2012). *Estimation des conditions de visibilité météorologique par caméras routières*. Université Paris-Est.

Baker, K. D., & Nayar, S. K. (2003). Photometric Model of a Rain Drop. *Rain*. Retrieved from http://citeseerx.ist.psu.edu/viewdoc/summary?doi=?doi=10.1.1.137.6470

Barnum, P. C., Narasimhan, S., & Kanade, T. (2010). Analysis of rain and snow in frequency space. *International Journal of Computer Vision*, *86*(2-3), 256–274. https://doi.org/10.1007/s11263-008-0200-2

Barnum, P., Kanade, T., & Narasimhan, S. (2007). Spatio-Temporal Frequency Analysis for Removing Rain and Snow from Videos. In *Proceedings of the First International Workshop on Photometric Analysis For Computer Vision - PACV 2007*. Retrieved from http://hal.inria.fr/inria-00264716

Beard, K. V., & Chuang, C. (1987). A new model for the equilibrium shape of raindrops. *Journal of the Atmospheric Sciences*, *44*(11), 1509–1524.

Beier, K., & Gemperlein, H. (2004). Simulation of infrared detection range at fog conditions for enhanced vision systems in civil aviation. *Aerospace Science and Technology*, *8*(1), 63–71.

Bergot, T. (2016). Large-eddy simulation study of the dissipation of radiation fog. *Quarterly Journal of the Royal Meteorological Society*.

Bernardin, F., Bremond, R., Ledoux, V., Pinto, M., Lemonnier, S., Cavallo, V., & Colomb, M. (2014). Measuring the effect of the rainfall on the windshield in terms of visual performance. *Accident Analysis & Prevention*, *63*, 83–88.

Bhise, V. D., Meldrum, J. F., Forbes, L. M., Rockwell, T. H., & McDowell, E. D. (1981). Predicting driver seeing distance in natural rainfall. *Human Factors: The Journal of the Human Factors and Ergonomics Society*, *23*(6), 667–682.

Biral. (2016). www.biral.com › Products › Present Weather Sensors (accessed on 29/08/2016).

Blanco, M., & Hankey, J. (2005). *Enhanced Night Visibility Series: Phase II-Study 4: Visual Performance During Nighttime Driving in Fog*. FHWA-HRT-04.

Błaś, M., Sobik, M., Quiel, F., & Netzel, P. (2002). Temporal and spatial variations of fog in the Western Sudety Mts., Poland. *Atmospheric Research*, *64*(1), 19–28.

Brenguier, J.-L., Bourrianne, T., Coelho, A. A., Isbert, J., Peytavi, R., Trevarin, D., & Weschler, P. (1998). Improvements of droplet size distribution measurements with the Fast-FSSP (Forward Scattering Spectrometer Probe). *Journal of Atmospheric and Oceanic Technology*, *15*(5), 1077–1090.

Burnet, F., Gomes, L., Haeffelin, M., Dupont, J., & Elias, T. (2012). Analysis of the microphysical structures of fog during the ParisFog project. In *Proceedings of the 16th international conference of clouds and precipitation (ICCP), Leipzig, Germany* (Vol. 30, p. 582).

Campbell. (2016). http://www.campbellsci.co.uk/index.cfm?cid=5&id=2.

Carvalho, S. C. P., de Lima, J. L. M. P., & de Lima, M. I. P. (2014). Using meshes to change the characteristics of simulated rainfall produced by spray nozzles. *International Soil and Water Conservation Research*, *2*(2), 67–78. https://doi.org/10.1016/S2095-6339(15)30007-1

Cermak, J., & Bendix, J. (2011). Detecting ground fog from space–a microphysics-based approach. *International Journal of Remote Sensing*, *32*(12), 3345–3371.

Cermak, J., Eastman, R. M., Bendix, J., Warren, S. G., & others. (2009). European climatology of fog and low stratus based on geostationary satellite observations. *Quarterly Journal of the Royal Meteorological Society*, *135*(645), 2125–2130.

Chowdhury, M. N., Testik, F. Y., Hornack, M. C., & Khan, A. A. (2016). Free fall of water drops in laboratory rainfall simulations. *Atmospheric Research*, *168*, 158–168. https://doi.org/10.1016/j.atmosres.2015.08.024

Cimel. (2016). http://www.cimel.fr/.

Claassens, A. S., & van der Watt, H. v. H. (1993). An inexpensive, portable rain simulator: construction and test data. *South African Journal of Plant and Soil*, *10*(1), 6–11. https://doi.org/10.1080/02571862.1993.10634635

Cohen, A. S., & Fischer, H. (1988). Does the windshield wiper impede a driver's vision? *International Journal of Vehicle Design*, *9*(4-5), 533–541.

Colomb, M., Hirech, K., André, P., Boreux, J. J., Lacôte, P., & Dufour, J. (2008). An innovative artificial fog production device improved in the European project "FOG." *Atmospheric Research*, *87*(3-4), 242–251. https://doi.org/10.1016/j.atmosres.2007.11.021

Crosby, J. D. (2003). Visibility sensor accuracy: what's realistic. In *12th Symposium on Meteorological Observations and Instrumentation, Long Beach, CA* (Vol. 13).

Dahmane, K., Duthon, P., Chausse, F., Bernardin, F., Colomb, M., & Essouri Ben Amara, N. (2016). The Cerema database : A specific

pedestrian detectors. proceedings of the international conference on Sciences of Electronics, Technologies of Information and Telecommunications, SETIT2016, Hammamet 18-20 dec. 2016.

Degefie, D., El-Madany, T.-S., Hejkal, J., Held, M., Dupont, J.-C., Haeffelin, M., & Klemm, O. (2015). Microphysics and energy and water fluxes of various fog types at SIRTA, France. *Atmospheric Research*, *151*, 162–175.

Degreane Horizon. (2016). http://www.degreane-horizon.com/.

Desaulniers-Soucy, N., Lovejoy, S., & Schertzer, D. (2001). The HYDROP experiment: An empirical method for the determination of the continuum limit in rain. *Atmospheric Research*, *59-60*, 163–197. https://doi.org/10.1016/S0169-8095(01)00115-6

Dumas, G., & Lemay, J. (2004). Splash and spray measurement and control: Recent progress in quebec. In *The Aerodynamics of Heavy Vehicles: Trucks, Buses, and Trains* (pp. 533–547). Springer.

Dumont, E. (2002). *Caractérisation, modélisation et simulation des effets visuels du brouillard pour l'usager de la route*. Université René Descartes-Paris V.

Dunne, T., Dietrich, W. E., & Brunengo, M. J. (1980). Simple, portable equipment for erosion experiments under artificial rainfall. *Journal of Agricultural Engineering Research*, *25*(2), 161–168. https://doi.org/10.1016/0021-8634(80)90057-8

Dupont, J.-C., Haeffelin, M., Protat, A., Bouniol, D., Boyouk, N., & Morille, Y. (2012). Stratus–fog formation and dissipation: a 6-day case study. *Boundary-Layer Meteorology*, *143*(1), 207–225.

Dupont, J., Haeffelin, M., Stolaki, S., & Elias, T. (2016). Analysis of dynamical and thermal processes driving fog and quasi-fog life cycles using the 2010–2013 ParisFog dataset. *Pure and Applied Geophysics*, *173*(4), 1337–1358.

Dye, J. E., & Baumgardner, D. (1984). Evaluation of the forward scattering spectrometer probe. Part I: Electronic and optical studies. *Journal of Atmospheric and Oceanic Technology*, *1*(4), 329–344.

Egli, S., Maier, F., Bendix, J., & Thies, B. (2015). Vertical distribution of microphysical properties in radiation fogs—A case study. *Atmospheric Research*, *151*, 130–145.

Elias, T., Dupont, J.-C., Hammer, E., Hoyle, C., Haeffelin, M., Burnet, F., & Jolivet, D. (2015). Enhanced extinction of visible radiation due to hydrated aerosols in mist and fog. *Atmospheric Chemistry and Physics*, *15*(12), 6605–6623.

Elias, T., Haeffelin, M., Drobinski, P., Gomes, L., Rangognio, J., Bergot, T., … Colomb, M. (2009). Particulate contribution to extinction of visible radiation: pollution, haze, and fog. *Atmospheric Research*, *92*(4), 443–454.

Esteves, M., Planchon, O., Lapetite, J. M., Silvera, N., & Cadet, P. (2000). The "EMIRE" large rainfall simulator: design and field testing. *Earth Surface Processes and Landforms*, *25*(7), 681–690. https://doi.org/10.1002/1096-9837(200007)25:7<681::AID-ESP124>3.0.CO;2-8

Eugster, W., Burkard, R., Holwerda, F., Scatena, F. N., & Bruijnzeel, L. S. (2006). Characteristics of fog and fogwater fluxes in a Puerto Rican elfin cloud forest. *Agricultural and Forest Meteorology*, *139*(3), 288–306.

Feingold, G., & Levin, Z. (1986). The lognormal fit to raindrop spectra from frontal convective clouds in Israel. *Journal of Climate and Applied Meteorology*, *25*(10), 1346–1363.

FOG Report. (2003). *FOG - European project "Improvement of transport safety by control of fog production in a chamber" GROWTH contract n° G6RD-CT-2000-00211 – 2000-2003- WP1 - "Project preparation in the different domains covered by the proposal."*

Foote, G., & Toit, P. D. (1969). Terminal velocity of raindrops aloft. *Journal of Applied Meteorology*. Retrieved from http://journals.ametsoc.org/doi/abs/10.1175/1520-0450(1969)008<0249:TVORA>2.0.CO;2

Garg, K., & Nayar, S. (2004). Detection and removal of rain from videos. *\ldots and Pattern Recognition, 2004. CVPR 2004 \ldots*. Retrieved from http://ieeexplore.ieee.org/xpls/abs_all.jsp?arnumber=1315077

Garg, K., & Nayar, S. (2006). Photorealistic rendering of rain streaks. *ACM Transactions on Graphics (TOG)*. Retrieved from http://dl.acm.org/citation.cfm?id=1141985

Garg, K., & Nayar, S. K. (2007). Vision and Rain. *International Journal of Computer Vision*, *75*(1), 3–27. https://doi.org/10.1007/s11263-006-0028-6

Gerber, H. (1991). Direct measurement of suspended particulate volume concentration and far-infrared extinction coefficient with a laser-diffraction instrument. *Applied Optics*, *30*(33), 4824–4831.

Gerber, H., Arends, B., & Ackerman, A. (1994). New microphysics sensor for aircraft use. *Atmospheric Research*, *31*(4), 235–252.

Giulianelli, L., Gilardoni, S., Tarozzi, L., Rinaldi, M., Decesari, S., Carbone, C., ... Fuzzi, S. (2014). Fog occurrence and chemical composition in the Po valley over the last twenty years. *Atmospheric Environment*, *98*, 394–401.

Glickman, T. S., & Zenk, W. (2000). Glossary of meteorology.

Green, M. (2008). *Forensic vision with application to highway safety*. Lawyers & Judges Publishing Company.

Gultepe, I., Müller, M., & Boybeyi, Z. (2006). A new visibility parameterization for warm-fog applications in numerical weather prediction models. *Journal of Applied Meteorology and Climatology*, *45*(11), 1469–1480.

Gultepe, I., Pearson, G., Milbrandt, J., Hansen, B., Platnick, S., Taylor, P., ... Cober, S. (2009). The fog remote sensing and modeling field project. *Bulletin of the American Meteorological Society*, *90*(3), 341.

Gultepe, I., Tardif, R., Michaelides, S., Cermak, J., Bott, A., Bendix, J., ... others. (2007). Fog research: A review of past achievements and future perspectives. *Pure and Applied Geophysics*, *164*(6-7), 1121–1159.

Gunn, R., & Kinzer, G. (1949). The terminal velocity of fall for water droplets in stagnant air. *Journal of Meteorology*. Retrieved from http://journals.ametsoc.org/doi/abs/10.1175/1520-0469(1949)006<0243:TTVOFF>2.0.CO;2

Guyot, G., Gourbeyre, C., Febvre, G., Shcherbakov, V., Burnet, F., Dupont, J.-C., … Jourdan, O. (2015). Quantitative evaluation of seven optical sensors for cloud microphysical measurements at the Puy-de-Dôme Observatory, France. *Atmospheric Measurement Techniques*, *8*(10), 4347–4367.

Haeffelin, M., Bergot, T., Elias, T., Tardif, R., Carrer, D., Chazette, P., … others. (2010). PARISFOG: shedding new light on fog physical processes. *Bulletin of the American Meteorological Society*, *91*(6), 767–783.

Haeffelin, M., Dupont, J., Boyouk, N., Baumgardner, D., Gomes, L., Roberts, G., & Elias, T. (2013). A Comparative Study of Radiation Fog and Quasi-Fog Formation Processes During the ParisFog Field Experiment 2007. *Pure and Applied Geophysics*, *170*(12), 2283–2303. https://doi.org/10.1007/s00024-013-0672-z

Hautière, N., Bigorgne, E., & Aubert, D. (2008). Daytime visibility range monitoring through use of a roadside camera. In *2008 IEEE Intelligent Vehicles Symposium* (pp. 470–475). IEEE. https://doi.org/10.1109/IVS.2008.4621200

Hautiere, N., Labayrade, R., & Aubert, D. (2006). Estimation of the visibility distance by stereovision: A generic approach. *IEICE Transactions on Information and Systems*, *E89-D*(7), 2084–2091. https://doi.org/10.1093/ietisy/e89-d.7.2084

Hautière, N., Tarel, J.-P., Lavenant, J., & Aubert, D. (2006). Automatic fog detection and estimation of visibility distance through use of an onboard camera. *Machine Vision and Applications*, *17*(1), 8–20. https://doi.org/10.1007/s00138-005-0011-1

Heintzenberg, J. (1994). Properties of the log-normal particle size distribution. *Aerosol Science and Technology*, *21*(1), 46–48.

Holejko, K., & Nowak, R. (1997). Fog detection and visibility measurements using forward scattered radiation. *Opto-Electronics Review Wol*, *5*.

Horvath, H., & Noll, K. E. (1969). The relationship between atmospheric light scattering coefficient and visibility. *Atmospheric Environment (1967)*, *3*(5), 543–550.

Huang, J., Tan, H.-S., & Bu, F. (2010). Immediate Manual-Automatic Vehicle Control Transitions based on Dynamic Initial Conditioning. *IFAC Proceedings Volumes*, *43*(18), 492–498.

Hu, Y., & Stamnes, K. (1993). An accurate parameterization of the radiative properties of water clouds suitable for use in climate models. *Journal of Climate*, *6*(4), 728–742.

Iserloh, T., Ries, J. B., Arnáez, J., Boix-Fayos, C., Butzen, V., Cerdà, A., … Wirtz, S. (2013). European small portable rainfall simulators: A comparison of rainfall characteristics. *CATENA*, *110*, 100–112. https://doi.org/10.1016/j.catena.2013.05.013

Ivey, D. L., Griffin III, L., Wambold, J., Zimmer, R., & Ross Jr, H. (1984). Influence of roadway surface discontinuities on safety. *NTIS, SPRINGFIELD, VA(USA). 1984*.

Ivey, D. L., Lehtipuu, E. K., & Button, J. W. (1975). *Rainfall and visibility - the view from behind the wheel* (p. 51). Texas Transportation Institute, Texas A & M University (College Station). Retrieved from http://www.getcited.org/pub/101655443

Kathiravelu, G., Lucke, T., & Nichols, P. (2016). Rain Drop Measurement Techniques: A Review. *Water*, *8*(2), 29. https://doi.org/10.3390/w8010029

Khlystou, A., Kos, G. P. A., & ten Brink, H. M. (1996). A High-Flow Turbulent Cloud Chamber. *Aerosol Science and Technology*, *24*(2), 59–68. https://doi.org/10.1080/02786829608965352

Klein, L. A. (1997). *Millimeter Wave and Infrared Multisensor Design and Signal Processing*. Artech House, Inc.

Klemm, O., & Lin, N.-H. (2016). What Causes Observed Fog Trends: Air Quality or Climate Change? *Aerosol and Air Quality Research*, *16*(5), 1131–1142.

Koračin, D., Dorman, C. E., Lewis, J. M., Hudson, J. G., Wilcox, E. M., & Torregrosa, A. (2014). Marine fog: A review. *Atmospheric Research*, *143*, 142–175.

Kumar, A., & Sudipta, T. (2012). Removal of rain from videos : a review. h
012-0373-6

Kunkel, B. A. (1984). Parameterization of droplet terminal velocity and extinction coefficient in fog models. *Journal of Climate and Applied Meteorology*, *23*(1), 34–41.

Lance, S., Brock, C., Rogers, D., & Gordon, J. (2010). Water droplet calibration of the Cloud Droplet Probe (CDP) and in-flight performance in liquid, ice and mixed-phase clouds during ARCPAC. *Atmospheric Measurement Techniques*, *3*(6), 1683–1706.

Lassu, T., Seeger, M., Peters, P., & Keesstra, S. D. (2015). The Wageningen Rainfall Simulator: Set-up and Calibration of an Indoor Nozzle-Type Rainfall Simulator for Soil Erosion Studies: THE WAGENINGEN RAINFALL SIMULATOR. *Land Degradation & Development*, *26*(6), 604–612. https://doi.org/10.1002/ldr.2360

Li, C., & Peng, P. (2012). Visibility measurement using multi-angle forward scattering by liquid droplets. *Measurement Science and Technology*, *23*(10), 105802.

Liou, K.-N. (2002). *An introduction to atmospheric radiation* (Vol. 84). Academic press.

Löffler-Mang, M., & Joss, J. (2000). An optical disdrometer for measuring size and velocity of hydrometeors. *Journal of Atmospheric and Oceanic Technology*, *17*(2), 130–139.

Marshall, J., & Palmer, W. (1948). The distribution of raindrops with size. *Journal of Meteorology*. Retrieved from http://journals.ametsoc.org/doi/abs/10.1175/1520-0469(1948)005<0165:TDORWS>2.0.CO;2

Mazoyer, M. (2016). *Impact du processus d'activation sur les propriétés microphysiques des brouillards et sur leur cycle de vie*.

Molinié, G., Desvignes, M., Courgeon, L., Mora, H., Mercier, B., & Gérard, S. (2016). A single video camea disdrometer (SCD) imaging raindrops at a resolution of 10 seconds or less, under publication. *LTHE, Université de Grenoble/CNRS*.

Morin, J., Cluff, C., & Powers, W. (1970). Realistic rainfall simulation for field investigation.

Muhammad, S. S., Flecker, B., Leitgeb, E., & Gebhart, M. (2007). Characterization of fog attenuation in terrestrial free space optical links. *Optical Engineering*, *46*(6), 066001–066001.

Nakanishi, M. (2000). Large-eddy simulation of radiation fog. *Boundary-Layer Meteorology*, *94*(3), 461–493.

Nielsen, C. B., Bendtsen, H., Andesen, B., & Larsen, H. E. (1999). Noise Reducing Pavements in Japan.

OECD. (1976). *Adverse Weather, Reduced Visibility and Road Safety*. Paris, France: (Organization for Economic Cooperation and Development) Research Group.

Paschkewitz, J. S. (2006). *Simulation of spray dispersion in a simplified heavy vehicle wake*. Lawrence Livermore National Laboratory.

Price, J. (2011). Radiation fog. Part I: observations of stability and drop size distributions. *Boundary-Layer Meteorology*, *139*(2), 167–191.

Public Work Research Institute. (1998). *PWRI "AHS Development Testing Using Weather Environment test Track."* Japon: Ministry of construction.

Rabiei, E., Haberlandt, U., Sester, M., & Fitzner, D. (2013). Rainfall estimation using moving cars as rain gauges - laboratory experiments. *Hydrology and Earth System Sciences*, *17*(11), 4701–4712. https://doi.org/10.5194/hess-17-4701-2013

Radovich, C. A. (2010). *EXPERIMENTS ON SPRAY FROM A ROLLING TIRE*. FACULTY OF THE GRADUATE SCHOOL UNIVERSITY OF SOUTHERN CALIFORNIA.

Renard, J.-B., Dulac, F., Berthet, G., Lurton, T., Vignelles, D., Jégou, F., … others. (2016). LOAC: a small aerosol optical counter/sizer for ground-based and balloon measurements of the size distribution and nature of atmospheric particles–Part 1: Principle of measurements and instrument evaluation. *Atmospheric Measurement Techniques*, *9*(4), 1721–1742.

Rodgers, G., Poots, G., Page, J., & Pickering, W. (1974). Theoretical predictions of raindrop impaction on a slab type building. *Building Science*, *9*(3), 181–190.

Rogers, R., & Yau, M. K. (1996). *A short course in cloud physics*. Elsevier.

Sachweh, M., & Koepke, P. (1995). Radiation fog and urban climate. *Geophysical Research Letters*, *22*(9), 1073–1076.

Scherrer, S. C., & Appenzeller, C. (2014). Fog and low stratus over the Swiss Plateau- a climatological study. *International Journal of Climatology*, *34*(3), 678–686.

Shehata, M. S., Cai, J., Badawy, W. M., Burr, T. W., Pervez, M. S., Johannesson, R. J., & Radmanesh, A. (2008). Video-Based Automatic Incident Detection for Smart Roads : The Outc Challenges Regarding False Alarms, *9*(2), 349–360.

Singh, V. P. (2011). Experimental Study of the Effects of Environmental and Fog Condensation Nuclei Parameters on the Rate of Fog Formation and Dissipation Using a New Laboratory Scale Fog Generation Facility. *Aerosol and Air Quality Research*. https://doi.org/10.4209/aaqr.2010.08.0071

Siogkas, G. K., & Dermatas, E. S. (2006). Detection, Tracking and Classification of Road Signs in Adverse Conditions. *MELECON 2006 - 2006 IEEE Mediterranean Electrotechnical Conference*, 537–540. https://doi.org/10.1109/MELCON.2006.1653157

Spiegel, J., Zieger, P., Bukowiecki, N., Hammer, E., Weingartner, E., & Eugster, W. (2012). Evaluating the capabilities and uncertainties of droplet measurements for the fog droplet spectrometer (FM-100). *Atmospheric Measurement Techniques*, *5*(9), 2237–2260.

Tampieri, F., & Tomasi, C. (1976). Size distribution models of fog and cloud droplets in terms of the modified gamma function. *Tellus*, *28*(4), 333–347.

Tardif, R., & Rasmussen, R. M. (2007). Event-based climatology and typology of fog in the New York City region. *Journal of Applied Meteorology and Climatology*, *46*(8), 1141–1168.

Thies Clima. (2016). http://www.thiesclima.com/ind1e.html.

Tokay, A., & Beard, K. V. (1995). A field study of raindrop oscillations. *American Meteorological Society*, 1671–1687.

Tombach, I., & Allard, D. (1980). Intercomparison of visibility measurement methods. *Journal of the Air Pollution Control Association*, *30*(2), 134–142.

Tripathi, A., & Mukhopadhyay, S. (2011). A Probabilistic Approach for Detection and Removal of Rain from Videos. *IETE Journal of Research*, *57*(1), 82. https://doi.org/10.4103/0377-2063.78382

Ulbrich, C. W. (1983). Natural variations in the analytical form of the raindrop size distribution. *Journal of Climate and Applied Meteorology*, *22*(10), 1964–1775.

Vaisala. (2015). Transmitter WXT510 with the Vaisala RAINCAP® Sensor. 2012, 1. Available online: www.vaisala.com (accessed on 15 June 2015).

Vaisala. (2016). http://www.vaisala.fr/.

Vajda, A., Tuomenvirta, H., Jokinen, P., Luomaranta, A., Makkonen, L., Tikanmäki, M., ... others. (2011). Probabilities of adverse weather affecting transport in Europe: climatology and scenarios up to the 2050s. *FMI Reports*, *9*, 85.

Van Mook, F. J. R., Wit, M. H. D., & Wisse, J. A. (1997). COMPUTER SIMULATION OF DRIVING RAIN ON BUILDING ENVELOPES. In *2nd European and African Conference on Wind Engineering* (pp. 22–26).

Van Oldenborgh, G. J., Yiou, P., & Vautard, R. (2010). On the roles of circulation and aerosols in the decline of mist and dense fog in Europe over the last 30 years. *Atmospheric Chemistry and Physics*, *10*(10), 4597–4609.

Vautard, R., Yiou, P., & van Oldenborgh, G. J. (2009). Decline of fog, mist and haze in Europe over the past 30 years. *Nature Geoscience*, *2*(2), 115–119.

Villermaux, E., & Eloi, F. (2011). The distribution of raindrops speeds, *38*(July), 10–13. https://doi.org/10.1029/2011GL048863

Virginia Tech Transportation Institute. (2016). *Virginia Smart Road*.

Wang, J., Liu, X., Yang, X., Lei, M., Ruan, S., Nie, K., ... Liu, J. (2014). Development and evaluation of a new digital photography visiometer system for automated visibility observation. *Atmospheric Environment*, *87*, 19–25.

WMO. (2016). (World Meteorological Organisation), Meteoterm terminology database. url: http://wmo.multicorpora.net/MultiTransWeb/Web.mvc.

Wong, K. (2012). Performance of several present weather sensors as precipitation gauges. *WMO TECO*, 16–18.

Yamawaki, T., Yamano, S., Katogi, Y., Tamura, T., & Ohira, Y. (2000). Millimeter-wave obstacle detection radar. *FUJITSU Ten*, *15*(15), 10–22.

Zhou, B., & Ferrier, B. S. (2008). Asymptotic analysis of equilibrium in radiation fog. *Journal of Applied Meteorology and Climatology*, *47*(6), 1704–1722.

Zwahlen, H. (1980). Driver Eye Scanning Behavior in Rain and During Unexpected Windshield Wiper Failure. *Z VERKEHRSSICHERHEIT*, *26*(4).

Glossary

Abbreviation	Definition
ABS	Anti-lock Braking System
ACC	Adaptive Cruise Control
ADAS	Advanced Driver Assistance Systems
ADC	Analog to Digital Converter
ASIC	Specific Integrated Circuit
BOM	Bill of Material
BSD	Blind Spot Detection
CA	Consortium Agreement
CNN	Convolutional Neural Networks
CW	Continuous Wave
DBF	Digital Beam Forming
DSD	Drop Size Distributions
ECU	Electronic Control Unit
FIR	Far Infrared
FMCW	Frequency Modulated Continuous Wave
FMEA	Failure Mode and Effects Analysis
FMEA	Failure Mode and Effects Analysis
FP	Framework Program
FPGA	Field-Programmable Gate Array
GA	General Assembly
GDP	Gross Domestic Product
GPU	Graphics Processing Units
GSM	Global System for Mobile Communications
HW	Hardware
ICT	Information and Communication Technologies
IM	Innovation Manager
InGaAs	Indium Gallium Arsenide
IPR	Intellectual Property Right
IR	Infrared
ISM	Industrial, Scientific and Medical

Abbreviation	Definition
IVSS	Intelligent Vehicle Safety Systems
LWIR	Long Wave Infrared
LWC	Liquid Water Content
MIMO	Multiple Input-Multiple Output
MMIC	Monolithic Microwave Integrated Circuit
MWIR	Mid Wave Infrared
NB	Narrow Band
NHTSA	National Highway Traffic Safety Association (in USA)
NIR	Near Infrared
PCB	Printed Circuit Boards
PDA	Photo-Diode Array
PMT	Project Management Team
PWRI	Public Works Research Institute
PWT22	Present Weather Detectors
R&D	Research and Development
RF	Radio Frequency
ROIC	Readout Integrated Circuit
RX	Receiver
SC	Semiconductor
S/N ratio	Signal/Noise Ratio
SoA	State of the Art
SMS	System Module Supplier
SPC	Single Particle Counters
SWIR	Short Wave Infrared
TEC	Thermoelectric
TRL	Technology Readiness Level
TX	Transmitter
UWB	Ultra Wide Band
VRU	Vulnerable Road User
WP	Work Package
WPL	Work Package Leader